

Supplementary Information

Contents

Appendix S1. Methods for reconstruction of <i>DBH</i>	2
Barro Colorado Island, Panama	2
Appendix S2. Methods for reconstruction of <i>DBH</i>	3
Appendix S3. Methods for climate data evaluation and correction	4
Appendix S4. Methods for comparing climwin results with traditional methods	5
Appendix S5. Dealing with rapidly changing climate and tree growth	7
Table S1. Site Details.	8
Table S2. Species analyzed, their characteristics, and bark allometries applied.	9
Table S3. Sampling details for species by site.	11
Table S4. Allometric equations for bark thickness.	12
Table S5. Qualitative comparison of results from this study with previous studies employing conventional methods.	13
Figure S1. Comparison of our approach with traditional methods of identifying climate signals: LITU at SCBI.	16
Figure S2. Comparison of our approach with traditional methods of identifying climate signals: ABAL at Zofin.	17
Figure S3. Comparison of our approach with traditional methods of identifying climate signals: PSME at Cedar Breaks.	18
Figure S4. Comparison of our approach with traditional methods of identifying climate signals: PIMA at Scotty Creek.	19
Figure S5. (PRE at SCBI)	20
Figure S6. (PET at SCBI)	21
Figure S7. (TMP/TMN at BCI)	22
Figure S9. Best GLS models for Barro Colorado Island (Panama)	23
Figure S10. Best GLS models for Huai Kha Khaeng (Thailand)	24
Figure S11. Best GLS models for the Smithsonian Conservation Biology Institute (Virginia, USA)	25
Figure S12. Best GLS models for Lilley Dickey Woods (Indiana, USA)	26
Figure S13. Best GLS models for Harvard Forest (Massachusetts, USA)	27
Figure S14. Best GLS models for Zofin Forest (Czech Republic)	28
Figure S15. Best GLS models for Niobrara/ Halsey (Nebraska, USA)	29
Figure S16. Best GLS models for Little Tesuque (New Mexico, USA)	30
Figure S17. Best GLS models for Cedar Breaks (Utah, USA)	31
Figure S18. Best GLS models for Scotty Creek (Northwest Territory, Canada)	32
SI References	33

Appendix S1. Methods for reconstruction of DBH

(include descriptions of stand history, global change dynamics)

Barro Colorado Island, Panama

Appendix S2. Methods for reconstruction of DBH

This is still rough/ mostly notes.

In most cases, when a recent *DBH* measurement was available, *DBH* was reconstructed from the outside in. In cases where *DBH* was not available, but when we knew that the core hit pith or could reasonably estimate how far off it was based on the curvature of the rings (Applequist, 1958; Duncan, 1989), *DBH* was reconstructed from the inside out.

For each core, *DBH* can be reconstructed outside-in (based on recent *DBH*, subtracting growth recorded in tree rings) or inside-out (summing *RW* from the inside out,—only when core hit pith or distance to pith can be reliably estimated). We generally gave precedence to the outside-in approach. Specifically, when *DBH* was taken at the time of coring,

At some of our sites where *DBH* was not taken at the time of coring (*SCBI*), *DBH* measurements taken before or slightly after the time of coring could be used. (see issue #19 in *ForestGEO_dendro*) If before, ... If after... For all outside-in reconstructions, if a negative *DBH* was predicted...

When there were more than one cores for a tree, the *DBH* reconstructions from each core were averaged to produce a single estimate of the tree's *DBH* through time. When the start or end dates of the records from the cores differed, we extrapolated growth of the shorter core to match the years covered by the longer core. Specifically, to fill in years at the more recent end, we assumed that the average growth rate of the ten years prior to the missing records applied to the missing years. To fill in years at the beginning of the tree's lifespan, we likewise assumed that the ten years adjacent to the missing record applied to the missing years; however, if this yielded a negative *DBH* estimate for the earliest year in the reconstruction, we divided the existing minimum *DBH* by number of years missing and applied that value to each year. We note that these reconstructed growth records were used only for the reconstruction of *DBH* and were not included as response variables in any of our analyses.

In either case we need bark thickness—ideally allometries describing the relationship between *DBH* and bark thickness (Table S4). This is especially critical for thick-barked species. When bark thickness data were available, we generated allometries (issue #8 in *ForestGEO_dendro*)... lognormal model with intercept forced to zero: `lm(bark_depth.mm ~ -1 + log(dbh_no_bark.cm+1):bark_species, data = bark)`. When bark thickness data were not available, we used published bark allometries from other sources (Table S4)

Appendix S3. Methods for climate data evaluation and correction

For BCI, we calculated monthly PPT and PDF from daily precipitation readings made on BCI starting in 1929 (Paton, 2019).

Appendix S4. Methods for comparing climwin results with traditional methods

To test whether our methods gave similar results to traditional methods, we conducted qualitative comparisons of our results to previous studies based on the same cores (Table S5) and conducted a formal quantitative comparison for four species (Figs. S1-S4), as detailed below.

Qualitative comparison

For all species-site combinations, we reviewed previous studies characterizing the climate sensitivity of growth using conventional methods. In most cases, we were able to compare with previous studies from the same sites and sets of cores. When these were not available, we reviewed regional-level analyses believed to be representative of the site.

Results from previous studies were compiled alongside results from the climate-only model in this study (Table S5). Where previous studies examined numerous climate variables or time windows (e.g., Helcoski et al., 2019), we focus on those most relevant to our findings.

Beyond the methodological differences, original studies based on the same sets of cores varied from this one and from one another in factors including the exact set of cores analyzed, climate data sources, time frame of analysis, approaches to identifying candidate climate variables and windows (including whether this is done on a site or species level), methods for detrending and standardizing to build chronologies, and whether the effects of temperature and precipitation are considered separately (original studies) or additively (this study). To standardize for such differences, we selected a subset of species for a standardized quantitative comparison, as detailed below.

Quantitative comparison

We also conducted a formal comparison of our approach to conventional methods using identical tree-ring and climate data for four species: PSME (Cedar Breaks, Utah), ABAL (*Žofín*), PIMA (Scotty Creek), and LITU (SCBI; Figs. S1-S4). These species were selected for analysis because they have been well-studied in the past. For each species, we compared climate sensitivities for the top precipitation- and temperature-group variables, as identified in the main analysis.

Prior to analysis, data were prepared and cleaned as described in the Methods section, resulting in an identical set of records for input into each analysis. For the approach developed here, analysis was conducted as described in the Methods section, but with the *climwin* climate variable selection process limited to just the species of interest (as opposed to all species at the site), climate variables considered individually rather than additively, analysis of only first-order linear relationships, and with start date adjusted to match the conventional method (see below). Following the *climwin* analysis step, we extracted *beta* coefficients describing the slope of the relationship between climate and *RW*. *Beta* coefficients, along with their standard error, were obtained for each month within the analysis time frame (Table S1) and for the time window identified as optimal by *climwin*.

For the analysis using conventional methods, the ring-width series from each core was standardized via ARSTAN using a 2/3rds n spline, where n is the number of years in the series (Cook, 1985; Cook & Kairiukstis, 1990- citations in Helcoski). (The following italic text is self-plagiarized from Helcoski and needs to be reworded:) The influence of outliers in all series was reduced using the adaptive power transformation, which also stabilises the variance over time (Cook & Peters, 1997). Next, each series was stabilised using either the average correlation between raw ring-width series (*rbar*) method or a 1/3rds spline method to adjust changes in variance as series replication decreased towards the earlier portion of each chronology (Jones et al., 1997). The 1/3rds spline method was chosen when replication in the inner portion of each chronology (c. the inner 30–50 yr of each record depending on full chronology length) dropped below three trees. Once that step was complete, a robust biweight mean chronology for each species was calculated from the ring-width indices (Cook, 1985). We chose to use residual chronologies because the autoregressive standardisation process in creating them removes much of the tree-level autocorrelation in growth and these chronologies would most likely contain the most conservative information on drivers of interannual growth (Cook, 1985).

Following Helcoski et al. (2019), we defined chronology start dates according to the subsample signal strength (SSS), using a cutoff of SSS = 0.80 (or 80% of the population signal). Thus, for this analysis only, we defined

chronology start dates as the year the SSS exceeded 0.80 or two years after the start of the climate record, whichever came later. SSS exceeded 0.80 well before the start of the 1901 start of climate records for PSME (1800s), ABAL (1700), and PIMA (1850s). For LITU, SSS reached 0.8 with 11 trees in 1919, which we used as the start date for this series. We note that these start date criteria differ from those used in the main analysis (Table S3), which had earlier start dates because the analysis was not constrained by a need to represent the full population signal. End dates were defined as the last full year prior to sampling (Table S3).

Beta (slope) coefficients for the relationship between tree growth and the monthly climate variable were derived as in Helcoski et al. (2019): (*SELF-PLAGIARIZED CONTENT:*) *Analyses of climate-growth relationships were conducted using ‘dplR’ (Bunn, 2008) and ‘bootRes’ (Zang & Biondi, 2013), which correlated functions and bootstrapped confidence intervals for the relationships between annual growth and monthly climate variables following Biondi & Waikul (2004).* Pearson correlations between climate variables and tree-ring chronologies were converted to linear slopes using the method of Charney et al. (2016).

Finally, we generated plots comparing month-by-month *beta* coefficients describing climate sensitivity, and also comparing *beta* coefficients for the window identified as optimal by *climwin* Figs. S1-S4).

We note that despite designing the analyses to be as comparable as possible, one-to-one correspondence of *beta* coefficients is not necessarily expected for several reasons. First, although the analysis time frame is standardized between the two approaches, the relative influence of each year will generally vary between the two approaches. The traditional approach, which all cores into a single residual chronology with one value per year, gives equal weighting to each year. In contrast, under the approach developed here, the number records per year will vary across the analysis time frame, generally increasing over time as the younger trees enter the analysis. Thus, where many younger trees are included in the analysis, the two approaches will effectively give different weights to the years included in the analysis period. In cases where climate-sensitivity differs between old and young trees, or where the climate and/or climate response changed substantially over the analysis time frame (e.g., at Scotty Creek; Fig. S4; Sniderhan & Baltzer, 2016), this may lead to divergence of the climate sensitivities estimated by the two methods.

Second, traditional analysis methods (using ARSTAN) were primarily designed to distill population-level variation to obtain the strongest possible climate signal for the reconstruction of past climate (**Cook & Kariustis**), not to characterize climate responses on the individual level, where variation is inherently higher. While conversion of Pearson correlations to linear slopes *sensu* Charney et al. (2016) approximates climate responses, it does not provide an exact slope describing the relationship between individual-level or population mean growth and climate. This is because standardization of variance and averaging of individual-level residuals prior to the climate analysis fundamentally alters and obfuscates individual-level responses.

We suspect that both of these factors may underlie the tendency for the traditional method to estimate stronger climate sensitivity than the approach developed here for Scotty Creek (Fig. S4), a comprehensively sampled black spruce forest (i.e., including young trees) on melting permafrost. We note, however, that there are no statistically significant differences in the *beta* coefficients of the two approaches at this site.

Appendix S5. Dealing with rapidly changing climate and tree growth

ISSUE #25 in ForestGEO-climate-sensitivity

Our analysis included two sites where climate change has had pronounced effects on tree growth: Scotty Creek, NW Territories, Canada (SC) and Little Tesuque, New Mexico, USA (LT). At SC, rapidly rising temperatures are causing melting permafrost, summer moisture stress, resulting in negative growth trends in basal area index (*BAI*) starting around 1950 and significant growth declines since 1970 in 56% of trees (Sniderhan & Baltzer, 2016). At LT, increasingly warm drought has dramatically reduced growth (Williams et al., 2012), resulting in many missing rings in recent years.

Problematically, correlating tree growth residuals from which climate-driven trends had been removed against the climate signal with a strong directional trend would not necessarily identify the most relevant climate drivers.

For these sites, we experimented with three approaches to identifying the most important climate drivers (1) the method described above, (2) detrending the climate variables (**AT:prewhitening?**) prior to the climwin step, and (3) splitting analyses into decades before and after 1970 (*sensu* Sniderhan & Baltzer, 2016) (Appendix S5).

This is in process. We will try and compare 3 methods: (1) our standard approach, (2) detrending the climate variables (#53), (3) applying the climwin step only for older records--before the most rapid climate change. We will work with SC and LT researchers to determine which makes most sense, and use that as the main approach for these sites.

Table S1. Site Details.

site code	site name	latitude	longitude	elevation (m.a.s.l.)	cores within ForestGEO plot?	canopy positions	tree statuses	date range	dormant season*	months in climwin
BCI	Barro Colorado Island	9.15430	-79.8461	120-160	no	canopy	live, dead	1931-2014	Nov-Apr	pOct-cDec
HKK	Huai Kha Khaeng	15.63240	99.2170	549-638	no	all	live	1903-2011	Nov-Apr	pOct-cDec
SCBI	Smithsonian Conservation Biology Institute	38.89350	-78.1454	273-338	yes	all	live, dead	1903-2017	Oct-Apr	pMay-cAug
LDW	Lilly Dickey Woods	39.23590	-86.2181	230-303		canopy	live, dead	1903-2019		pMay-cAug
HF	Harvard Forest	42.53880	-72.1755	340-368	yes	all	live, dead	1903-2014		pMay-cAug
ZOF	Zofin Forest Dynamics Plot	48.66380	14.7073	736-829	some	all	live, dead	1903-2013	Oct-Mar	pMay-cAug
NE	Niobrara/Halsey	42.78000	-100.0210	644-702	some	canopy	live		Oct-Apr	pMay-cAug
LT	Little Tesuque	35.73838	-105.8382	2684 - 2702	n.a.	canopy / sub-canopy	live	1903-2018	Oct-Apr	pMay-cAug
CB	Utah Forest Dynamics Plot	37.66150	-112.8525	3020-3169	yes		live	1903-2007		pMay-cAug
SC	Scotty Creek	61.30000	-121.3000	280	no	all	live, dead	1903-2013	Sept-Apr	pMay-cAug

- Refers to approximate period during which woody growth ceases (dry season in the tropics, winter for temperate and boreal sites).

Table S2. Species analyzed, their characteristics, and bark allometries applied.

(ISSUE #72 in ForestGEO-climate-sensitivity)

NOTE: bark.allometry field is not yet right– we will have just one latin name per site, corresponding to allometries in Table S4. But it does give correct info for what is currently applied. We also intend to find and apply more allometries.

species code	family	latin name	sites sampled	leaf type	leaf phenology	light requirements	bark allometry
ABAL	Pinaceae	Abies alba	ZOF	needleleaf	evergreen	shade-tolerant	Abies lasiocarpa in Zofin
ABBI	Pinaceae	Abies bifolia	CB	needleleaf	evergreen		Abies lasiocarpa in CedarBreaks
ACRU	Sapindaceae	Acer rubrum	HF	broadleaf	deciduous (cold)		acru in HarvardForest
ACSA	Sapindaceae	Acer saccharum	LDW	broadleaf	deciduous (cold)		acru in LillyDickey, acru in LillyDickey
AFXY	Fabaceae	Afzelia xylocarpa	HKK	broadleaf	deciduous (drought)		neglected in HKK
BEAL	Betulaceae	Betula alleghaniensis	HF	broadleaf	deciduous (cold)		Betula alleghaniensis in HarvardForest
BEPA	Betulaceae	Betula papyrifera	NE	broadleaf	deciduous (cold)		Betula papyrifera in Nebraska
CACO	Juglandaceae	Carya cordiformis	SCBI	broadleaf	deciduous (cold)		caco in SCBI
CAGL	Juglandaceae	Carya glabra	SCBI	broadleaf	deciduous (cold)		cagl in SCBI
CAOV	Juglandaceae	Carya ovata	LDW	broadleaf	deciduous (cold)		cagl in LillyDickey
CAOVL	Juglandaceae	Carya ovalis	SCBI	broadleaf	deciduous (cold)		caovl in SCBI
CATO	Juglandaceae	Carya tomentosa	SCBI	broadleaf	deciduous (cold)		cato in SCBI
CHTA	Meliaceae	Chukrasia tabularis	HKK	broadleaf	brevi-deciduous (drought)		neglected in HKK
FAGR	Fagaceae	Fagus grandifolia	HF, SCBI	broadleaf	deciduous (cold)		neglected in HarvardForest, neglected in LillyDickey, neglected in SCBI
FASY	Fagaceae	Fagus sylvatica	ZOF	broadleaf	deciduous (cold)	shade-tolerant	neglected in Zofin
FRAM	Oleaceae	Fraxinus americana	LDW, SCBI	broadleaf	deciduous (cold)		fram in LillyDickey, fram in SCBI
FRNI	Oleaceae	Fraxinus nigra	SCBI	broadleaf	deciduous (cold)		fram in SCBI
JACO	Bignoniaceae	Jacaranda copaia	BCI	broadleaf	deciduous (drought)	light-demanding	JCO in BCI
JUNI	Juglandaceae	Juglans nigra	SCBI	broadleaf	deciduous (cold)		juni in SCBI
JUVI	Cupressaceae	Juniperus virginiana	NE	needleleaf	evergreen		neglected in Nebraska
LITU	Magnoliaceae	Liriodendron tulipifera	LDW, SCBI	broadleaf	deciduous (cold)		litu in LillyDickey, litu in SCBI
MEAZ	Meliaceae	Melia azedarach	HKK	broadleaf	deciduous (drought)	light-demanding	neglected in HKK
PIAB	Pinaceae	Picea abies	HF	needleleaf	evergreen	intermediate	Picea engelmannii in HarvardForest, Picea engelmannii in Zofin
PIEN	Pinaceae	Picea engelmannii	CB	needleleaf	evergreen		Picea engelmannii in CedarBreaks
PIFL	Pinaceae	Pinus flexilis	CB	needleleaf	evergreen		Pinus monticola in CedarBreaks
PILO	Pinaceae	Pinus longaeva	CB	needleleaf	evergreen		neglected in CedarBreaks
PIMA	Pinaceae	Picea mariana	SC	needleleaf	evergreen		PIMA in ScottyCreek
PIPO	Pinaceae	Pinus ponderosa	NE, LT	needleleaf	evergreen		Pinus jeffreyi in Little Tesuque, Pinus jeffreyi in Nebraska
PIPU	Pinaceae	Picea pungens	CB	needleleaf	evergreen		Picea engelmannii in CedarBreaks
PIST	Pinaceae	Pinus strobus	HF, SCBI	needleleaf	evergreen		Pinus strobus in HarvardForest, Pinus strobus in SCBI
POTR	Salicaceae	Populus tremuloides	CB	broadleaf	deciduous (cold)		Populus tremuloides in CedarBreaks
PSME	Pinaceae	Pseudotsuga menziesii	CB	needleleaf	evergreen		Pseudotsuga menziesii in CedarBreaks
QUAL	Fagaceae	Quercus alba	LDW, SCBI	broadleaf	deciduous (cold)		qual in LillyDickey, qual in SCBI
QUMO	Fagaceae	Quercus montana	LDW, SCBI	broadleaf	deciduous (cold)		qupr in LillyDickey, qupr in SCBI
QURU	Fagaceae	Quercus rubra	HF, LDW, SCBI	broadleaf	deciduous (cold)		quru in HarvardForest, quru in LillyDickey, quru in SCBI
QUVE	Fagaceae	Quercus velutina	LDW, SCBI	broadleaf	deciduous (cold)		quve in LillyDickey, quve in SCBI
TEPA	Burseraceae	Tetragastris panamensis	BCI	broadleaf	evergreen	shade-tolerant	TPA in BCI
TOCI	Meliaceae	Toona ciliata	HKK	broadleaf	deciduous (drought)		neglected in HKK
TRTU	Meliaceae	Trichilia tuberculata	BCI	broadleaf	evergreen	shade-tolerant	TTU in BCI
TSCA	Pinaceae	Tsuga canadensis	HF	needleleaf	evergreen		Tsuga canadensis in HarvardForest

*Bark allometry field indicates the species and site sampled to construct the bark allometry. When neither

raw data nor an allometric equation for the study species was available, we selected the most appropriate equation that could be located for similar species. Equations are given in Table S4.

Table S3. Sampling details for species by site.

(ISSUE #73 in ForestGEO-climate-sensitivity)

site	species code	n trees all	n cores all	n trees dbh	n cores dbh	dbh range sampled	dbh range reconstructed*	date range
BCI	JACO	12	18	11	17	30.2-63.5	2.6-56.4	1931-2014
BCI	TEPA	18	29	17	26	22.1-59.5	2.7-49.4	1931-2014
BCI	TRTU	23	37	20	31	20.7-43.6	4.8-41.5	1931-2014
CB	ABBI	22	41	20	37	13.9-54.2	0.6-45.3	1903-2000
CB	PIEN	12	21	10	16	14-54.9	3.6-39.4	1903-2000
CB	PIFL	12	19	11	18	17.6-63.5	4.5-55.4	1903-1998
CB	PILO	17	24	NA	NA	NA	NA	1903-1999
CB	PIPU	15	28	15	28	22.4-50.8	8.6-48.5	1903-2000
CB	POTR	17	27	17	27	23.6-47.6	7.7-42.4	1903-2000
CB	PSME	10	19	10	19	20.7-64.2	2.6-49.4	1903-1999
HF	ACRU	18	59	18	59	10.1-22.1	0.9-20.4	1903-2013
HF	BEAL	13	44	13	44	10.2-37.9	1.6-20.5	1904-2013
HF	QURU	74	180	73	177	19.5-53	1.1-48.3	1903-2014
HF	TSCA	32	83	32	82	10.6-37	0.6-33.5	1923-2014
HKK	AFXY	39	127	39	127	20.1-98.7	0.1-81.4	1903-2011
HKK	CHTA	28	70	28	70	16-64.6	0.2-59.5	1904-2010
HKK	MEAZ	46	130	46	130	25.6-98.1	3.8-80.3	1914-2011
HKK	TOCI	45	143	45	143	16.6-116.4	1.7-80.5	1903-2011
LDW	ACSA	35	66	34	64	9-64.6	0.5-2.4	1903-2019
LDW	CAOV	9	18	8	15	NA-NA	1.4-37.4	1903-2013
LDW	LITU	15	28	14	25	NA-NA	1.2-69.4	1903-2019
LDW	QUAL	10	20	NA	NA	NA	NA	1903-2013
LDW	QUMO	10	20	8	16	NA-NA	1.1-52.4	1903-2013
LDW	QUVE	9	18	NA	NA	NA	NA	1903-2013
NE	BEP A	28	84	28	84	NA-NA	0.4-30.5	1903-1995
NE	JUVI	29	60	29	60	16.6-21.5	1.6-18.4	1941-1994
NE	PIPO	59	114	57	110	19.3-63	1.8-46.9	1934-1994
LT	PIPO	10	20	10	20	23.2-52.8	14.6-48.4	1903-2018
LT	PIST2	7	14	7	13	25.7-39.8	4.2-34.4	1903-2018
SCBI	CACO	15	15	14	14	10.62-38.52	1.7-32.2	1903-2015
SCBI	CAGL	39	39	36	36	10.28-52.31	1.6-49.3	1903-2015
SCBI	CAOVL	25	25	24	24	15.11-60.32	2.6-47.2	1903-2015
SCBI	CATO	15	15	14	14	12.86-35.95	3.7-28.4	1903-2015
SCBI	FAGR	76	76	74	74	10.05-41.02	0.1-41.2	1920-2009
SCBI	FRAM	66	66	61	61	8.11-94.73	0.1-84.4	1903-2016
SCBI	FRNI	12	12	12	12	11.04-39.2	0.5-27.3	1903-1996
SCBI	JUNI	30	30	28	28	20.4-76.19	5.6-59.5	1903-2010
SCBI	LITU	106	106	104	104	10-91.42	0.1-81.1	1903-2010
SCBI	PIST	36	36	36	36	13.92-50.96	0.5-44.3	1931-2010
SCBI	QUAL	66	66	66	66	11.4-76.73	0.3-70.4	1903-2009
SCBI	QUMO	67	67	67	67	10.22-84.59	0.3-69.5	1903-2017
SCBI	QURU	70	70	70	70	11.07-87.65	2.5-79.2	1903-2016
SCBI	QUVE	81	81	81	81	16.02-82.33	0.5-78.4	1903-2009
SC	PIMA	442	442	101	101	7-14.9	0.5-12.5	1903-2013
ZOF	ABAL	46	46	41	41	50-121	21.1-107.4	1903-2010
ZOF	FASY	1369	1369	1358	1358	NA-NA	0.1-115.3	1903-2013
ZOF	PCAB	644	644	599	599	NA-NA	0.5-126.4	1903-2011

*Maximum reconstructed DBH's analyzed are less than maximum sampled DBH's because we discard size ranges with < 3 conspecific trees.

Table S4. Allometric equations for bark thickness.

species	equation	n	DBH.range.cm	site	source
<i>Abies alba</i>	$bark.mm = ((0.05 + 0.06 * (dbh.cm/2.54))/2) * 2.54$	NA		North America	Miles, Patrick D.; Smith, W. Brad. 2009.
<i>Acer pseudoplatanus</i>	$bark.mm = 0.619 * \log(dbh.cm + 1)$	10	8.2-39.6	SCBI	Anderson-Teixeira et al. (2015)
<i>Betula alleghaniensis</i>	$bark.mm = ((0.15 + 0.03 * (dbh.cm/2.54))/2) * 2.54$	NA		North America	Miles, Patrick D.; Smith, W. Brad. 2009.
<i>Betula papyrifera</i>	$bark.mm = ((0.13 + 0.05 * (dbh.cm/2.54))/2) * 2.54$	NA		North America	Miles, Patrick D.; Smith, W. Brad. 2009.
<i>Carya cordiformis</i>	$bark.mm = 0.793 * \log(dbh.cm + 1)$	9	5.9-68.2	SCBI	Anderson-Teixeira et al. (2015)
<i>Carya glabra</i>	$bark.mm = 1.035 * \log(dbh.cm + 1)$	8	19.1-78	SCBI	Anderson-Teixeira et al. (2015)
<i>Carya ovalis</i>	$bark.mm = 1.531 * \log(dbh.cm + 1)$	8	6.4-63.1	SCBI	Anderson-Teixeira et al. (2015)
<i>Carya tomentosa</i>	$bark.mm = 1.105 * \log(dbh.cm + 1)$	8	5-57.3	SCBI	Anderson-Teixeira et al. (2015)
<i>Fraxinus americana</i>	$bark.mm = 2.223 * \log(dbh.cm + 1)$	9	6.1-94.2	SCBI	Anderson-Teixeira et al. (2015)
<i>Jacaranda copaia</i>	$bark.mm = 2.993 * \log(dbh.cm + 1)$	5	45.6-75	Panama	Raquel Alfaro-Sánchez (unpublished data)
<i>Juglans nigra</i>	$bark.mm = 2.107 * \log(dbh.cm + 1)$	9	13.6-85.4	SCBI	Anderson-Teixeira et al. (2015)
<i>Liriodendron tulipifera</i>	$bark.mm = 1.637 * \log(dbh.cm + 1)$	9	27.5-136.5	SCBI	Anderson-Teixeira et al. (2015)
<i>Picea abies</i>	$bark.mm = ((0.15 + 0.04 * (dbh.cm/2.54))/2) * 2.54$	NA		North America	Miles, Patrick D.; Smith, W. Brad. 2009.
<i>Picea mariana</i>	$bark.mm = 3.726 * \log(dbh.cm + 1)$	12	6.9-7.9	Scotty Creek	Rajit Patankar and Jennifer Baltzer (unpublished data)
<i>Pinus flexilis</i>	$bark.mm = (1.299 * \sqrt{dbh.cm})^{0.609}^2$	29	10-130	California (3 montane sites)	Zeibig-Kichas et al. (2016)
<i>Pinus ponderosa</i>	$bark.mm = (1.298 * \sqrt{dbh.cm})^{0.802}^2$	81	5-160	California (4 montane sites)	Zeibig-Kichas et al. (2016)
<i>Pinus strobus</i>	$bark.mm = ((0.02 + 0.10 * (dbh.cm/2.54))/2) * 2.54$	NA		North America	Miles, Patrick D.; Smith, W. Brad. 2009.
<i>Populus tremuloides</i>	$bark.mm = ((0.10 + 0.07 * (dbh.cm/2.54))/2) * 2.54$	NA		North America	Miles, Patrick D.; Smith, W. Brad. 2009.
<i>Pseudotsuga menziesii</i>	$bark.mm = (0.785 * \sqrt{dbh.cm})^2$	30	10-200	California (3 montane sites)	Zeibig-Kichas et al. (2016)
<i>Pseudotsuga menziesii</i>	$bark.mm = ((0.40 + 0.17 * (dbh.cm/2.54))/2) * 2.54$	NA		North America	Miles, Patrick D.; Smith, W. Brad. 2009.
<i>Quercus alba</i>	$bark.mm = 1.828 * \log(dbh.cm + 1)$	10	9.3-101.8	SCBI	Anderson-Teixeira et al. (2015)
<i>Quercus montana</i>	$bark.mm = 2.083 * \log(dbh.cm + 1)$	8	5.8-99.1	SCBI	Anderson-Teixeira et al. (2015)
<i>Quercus rubra</i>	$bark.mm = 0.98 * \log(dbh.cm + 1)$	10	24.1-143.2	SCBI	Anderson-Teixeira et al. (2015)
<i>Quercus velutina</i>	$bark.mm = 1.394 * \log(dbh.cm + 1)$	8	16.2-110.7	SCBI	Anderson-Teixeira et al. (2015)
<i>Tetragastris panamensis</i>	$bark.mm = 1.672 * \log(dbh.cm + 1)$	4	22.7-48.8	Panama	Raquel Alfaro-Sánchez (unpublished data)
<i>Trichilia tuberculata</i>	$bark.mm = 1.367 * \log(dbh.cm + 1)$	12	21-40.5	Panama	Raquel Alfaro-Sánchez (unpublished data), Pete Kerby-Miller and Helene Muller-Landau (unpublished data)
<i>Tsuga canadensis</i>	$bark.mm = ((0.18 + 0.08 * (dbh.cm/2.54))/2) * 2.54$	NA		North America	Miles, Patrick D.; Smith, W. Brad. 2009.

For assignments of species as proxies for those with out available bark allometries, see Table S2.

Table S5. Qualitative comparison of results from this study with previous studies employing conventional methods.

species	Precipitation response		Temperature response		reference
	previously observed	observed here	previously observed	observed here	
Barro Colorado Island, Panama					
JACO	pos. correlation to Apr-Dec <i>PPT</i> (strongest of the 3 species)	pos. correlation to Mar-Dec <i>PPT</i> (strongest of the 3 species)	no sig. correlation to annual T_{mean} or T_{min}	neg. response to Feb-Mar T_{min}	Alfaro-Sánchez et al. 2017
TEPA	pos. correlation to Apr-Dec <i>PPT</i> (response weaker than JACO, similar to TRTU)	pos. correlation to Mar-Dec <i>PPT</i> (response weaker than JACO, similar to TRTU)	no sig. correlation to annual T_{mean} or T_{min}	no sig. correlation to Feb-Mar T_{min}	Alfaro-Sánchez et al. 2017
TRTU	pos. correlation to Apr-Dec <i>PPT</i> (response weaker than JACO, similar to TEPA)	pos. correlation to Mar-Dec <i>PPT</i> (response weaker than JACO, similar to TEPA)	no sig. correlation to annual T_{mean} or T_{min}	non-sig. slight pos. response to Feb-Mar T_{min}	Alfaro-Sánchez et al. 2017
Huai Kha Khaeng, Thailand					
AFXY	sig. pos. correlation with June <i>PPT</i> , otherwise n.s.	slight concave-down response to p.Sept-June <i>PPT</i> frequency	sig. neg. correlation with T_{max} in Aug and Dec; T_{min} in p.Oct., Jul, Aug	slight concave-down response to Apr-Oct T_{max}	Vlam et al. 2013
CHTA	sig. pos. correlation with April <i>PPT</i> , otherwise n.s.	slight concave-down response to p.Sept-June <i>PPT</i> frequency	sig. neg. correlation with T_{max} in May, Aug-Sept; T_{min} in Feb, May, Aug	slight neg. response to Apr-Oct T_{max}	Vlam et al. 2013
MEAZ	sig. pos. correlation with April <i>PPT</i> , otherwise n.s.	concave-down response to p.Sept-June <i>PPT</i> frequency	sig. neg. correlation with T_{max} in May-Aug; T_{min} in May-Aug	neg. response to Apr-Oct T_{max}	Vlam et al. 2013
TOCI	sig. pos. correlation with p.Oct-p.Nov and April-May <i>PPT</i>	concave-down /increasing response to p.Sept-June <i>PPT</i> frequency	sig. neg. correlation with T_{max} every month from pOct-June (excluding March); T_{min} in Jan and Mar-Aug	neg. response to Apr-Oct T_{max}	Vlam et al. 2013
Smithsonian Conservation Biology Institute, Virginia, USA					
CACO	pos. correlations with May-Aug <i>PPT</i> (sig. May, July)	neg. correlations with May-Aug <i>PET</i> (sig. May-July)	**(sig or ns)** neg. response to May-July <i>PET</i>	Helcoski et al. 2019	
CAGL	pos. correlations with May-Aug <i>PPT</i> (sig. May)	neg. correlations with May-Aug <i>PET</i> (n.s.)	**(sig or ns)** neg. response to May-July <i>PET</i>	Helcoski et al. 2019	
CAOVL	pos. correlations with May-Aug <i>PPT</i> (sig. Aug)	neg. correlations with May-Aug <i>PET</i> (sig. all months)	**(sig or ns)** neg. response to May-July <i>PET</i>	Helcoski et al. 2019	
CATO	pos. correlations with May-Aug <i>PPT</i> (n.s.)	neg. correlations with May-Aug <i>PET</i> (sig. June)	**(sig or ns)** neg. response to May-July <i>PET</i>	Helcoski et al. 2019	
FAGR	pos. correlations with May-Aug <i>PPT</i> (sig. July-Aug)	neg. correlations with May-Aug <i>PET</i> (sig. July-Aug)	**(sig or ns)** neg. response to May-July <i>PET</i>	Helcoski et al. 2019	
FRAM	pos. correlations with May-Aug <i>PPT</i> (sig. May-June)	neg. correlations with May-Aug <i>PET</i> (sig. May-June)	**(sig or ns)** neg. response to May-July <i>PET</i>	Helcoski et al. 2019	
FRNI	no sig. correlations with peak growing season <i>PPT</i>	no sig. correlations with peak growing season <i>PET</i>	**(sig or ns)** neg. response to May-July <i>PET</i>	Helcoski et al. 2019	
JUNI	pos. correlations with May-Aug <i>PPT</i> (sig. Jun-Aug)	neg. correlations with May-Aug <i>PET</i> (sig. July-Aug)	non-sig. neg. response to May-July <i>PET</i>	Helcoski et al. 2019	

S5, cont.

species	Precipitation response		Temperature response		reference
	previously observed	observed here	previously observed	observed here	
Smithsonian Conservation Biology Institute, Virginia, USA (cont.)					
LITU	pos. correlations with May-Aug <i>PPT</i> (sig. May-July)		neg. correlations with May-Aug <i>PET</i> (sig. all months)	**(sig or ns)** neg. response to May-July <i>PET</i>	Helcoski et al. 2019
PIST	pos. correlations with May-Aug <i>PPT</i> (n.s.)		neg. correlations with May-Aug <i>PET</i> (n.s.)	**(sig or ns)** neg. response to May-July <i>PET</i>	Helcoski et al. 2019
QUAL	pos. correlations with May-Aug <i>PPT</i> (sig. May)		neg. correlations with May-Aug <i>PET</i> (sig. all months)	**(sig or ns)** neg. response to May-July <i>PET</i>	Helcoski et al. 2019
QUMO	pos. correlations with May-Aug <i>PPT</i> (sig. May)		neg. correlations with May-Aug <i>PET</i> (sig. May-June, Aug)	**(sig or ns)** neg. response to May-July <i>PET</i>	Helcoski et al. 2019
QURU	pos. correlations with May-Aug <i>PPT</i> (n.s.)		neg. correlations with May-Aug <i>PET</i> (sig. May, July-Aug)	**(sig or ns)** neg. response to May-July <i>PET</i>	Helcoski et al. 2019
QUVE	pos. correlations with May-Aug <i>PPT</i> (sig. May-July)		neg. correlations with May-Aug <i>PET</i> (sig. all months)	**(sig or ns)** neg. response to May-July <i>PET</i>	Helcoski et al. 2019
Lilly Dickey Woods, Indiana, USA					
LITU	pos. correlations with Jun-Aug PDSI	pos. response to June <i>PPT</i>	neg. response to Jun-Aug <i>T_{max}</i>	neg. response to June <i>PET</i>	Maxwell, Harley, and Robeson 2016
QUAL	pos. correlations with Jun-Aug PDSI	pos. response to June <i>PPT</i>	neg. response to Jun-Aug <i>T_{max}</i>	neg. response to June <i>PET</i>	Maxwell, Harley, and Robeson 2016
QUMO	pos. correlations with Jun-Aug PDSI	pos. response to June <i>PPT</i>	neg. response to Jun-Aug <i>T_{max}</i>	neg. response to June <i>PET</i>	Maxwell, Harley, and Robeson 2016
QUVE	pos. correlations with Jun-Aug PDSI	pos. response to June <i>PPT</i>	neg. response to Jun-Aug <i>T_{max}</i>	neg. response to June <i>PET</i>	Maxwell, Harley, and Robeson 2016
Harvard Forest, Massachusetts, USA					
ACRU			no response to Jan- April <i>T_{min}</i> *	neg. correlation to Mar <i>PET</i>	Alexander et al. 2019
BEAL			no response to Jan- April <i>T_{min}</i> *	ns neg correlation with Mar <i>PET</i>	Alexander et al. 2019
QURU			no response to Jan- April <i>T_{min}</i> *	slight concave-down decreasing response to Mar <i>PET</i>	Alexander et al. 2019
TSCA			pos. response to Jan- April <i>T_{min}</i> *	pos. response to March <i>PET</i>	Alexander et al. 2019

S5, cont.

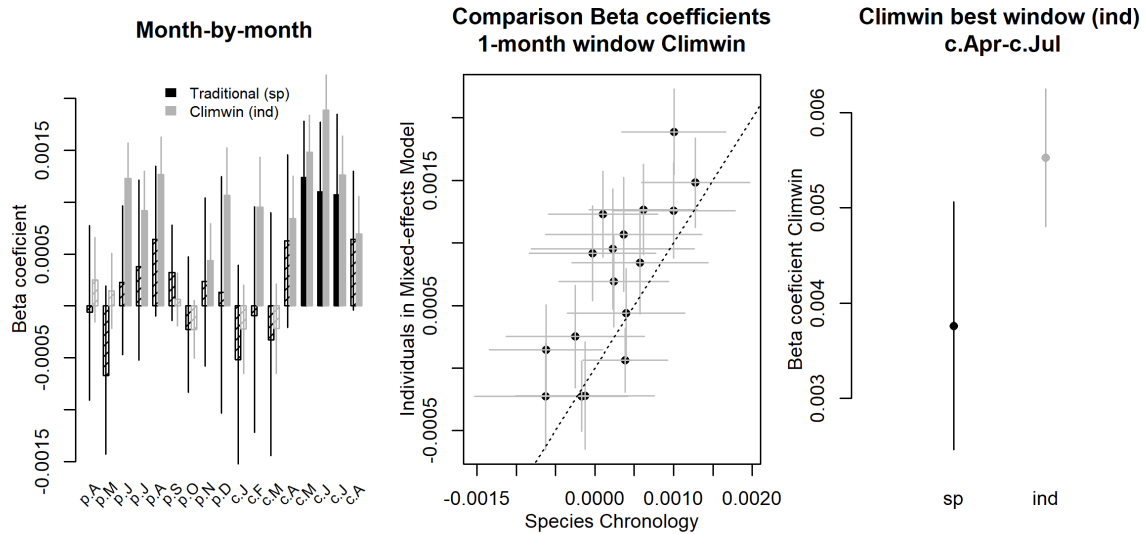
species	Precipitation response		Temperature response		reference
	previously observed	observed here	previously observed	observed here	
Žofín Forest Dynamics Plot, Czech Republic					
ABAL	no sig. correlations with June-July <i>PPT</i>	slight concave-down response to p.Jun-p.July <i>PPT</i> frequency	sig. pos. correlation to April T (strongest T correlation)	pos. response to Jan-March <i>T_{max}</i>	Kašpar, Tumajer, Vašíčková, and Šamonil, in review
FASY	no sig. correlations with June-July <i>PPT</i>	pos. response to p.Jun-p.July <i>PPT</i> frequency	sig. pos. correlation to Jan T (strongest T correlation)	pos. response to Jan-March <i>T_{max}</i>	Kašpar, Tumajer, Vašíčková, and Šamonil, in review
PIAB	modest pos. correlations (n.s) with June-July <i>PPT</i>	pos. response to p.Jun-p.July <i>PPT</i> frequency	sig. pos. correlation to March T (strongest current-year T correlation)	pos. response to Jan-March <i>T_{max}</i>	Kašpar, Tumajer, Vašíčková, and Šamonil, in review
Niobrara and Hansley, Nebraska, USA					
	>700m elev. sites moisture limited June-Aug		>700m elev. sites temperature limited except June-Aug		Tumajer et al. 2017
BEPA	little relationship to ppt within analysis timeframe (exception: pos. corr. with pAug pre); stronger relationship to streamflow and PDSI		little relationship to <i>T_{mean}</i> within analysis timeframe (exception: neg. corr. with pJune and cJan <i>T_{mean}</i>)		Bumann et al. 2019
JUVI	pos. correlations with <i>PPT</i> pJul-cJune		neg. correlation to cJun-cJul <i>T_{mean}</i>		Aus de Ar et al. 2018
PIPO	pos. correlations with <i>PPT</i> cApr-cAug		neg. correlation to <i>T_{mean}</i> in pJul, pSep, cMay, cJul		Aus de Ar et al. 2018
PIPO					Touchan et al., 2011 and Williams et al., 2013
PIST2					Touchan et al., 2011 and Williams et al., 2013
					-
					Sniderhan and Baltzer 2016

*Indicates results from a regional study including but not limited to cores from the focal site.

**Indicates results from a regional study not including the focal site, but believed to be representative.

Figure S1. Comparison of our approach with traditional methods of identifying climate signals: LITU at SCBI.

Precipitation



Potential Evapotranspiration

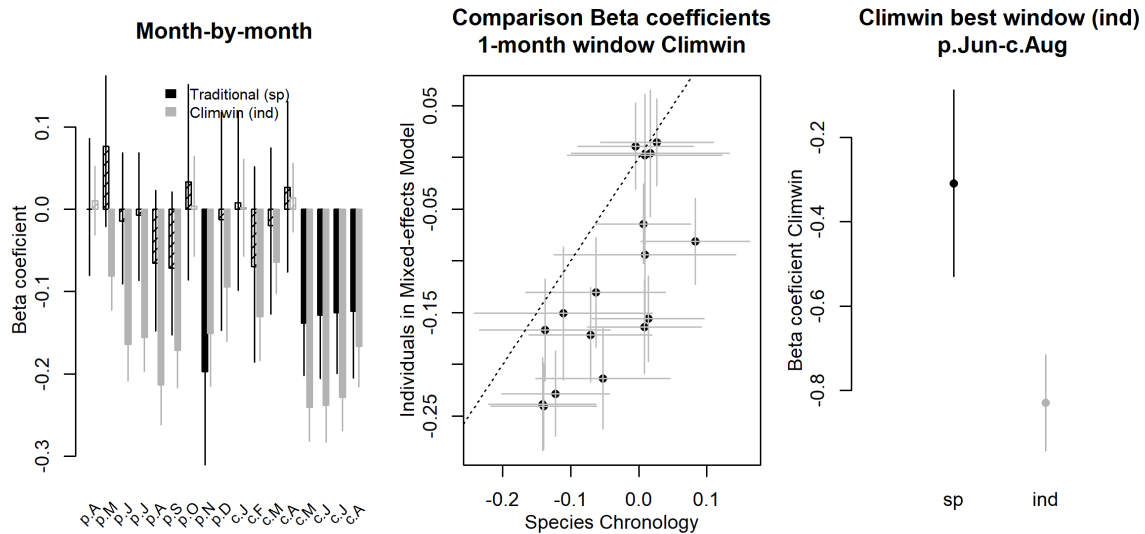
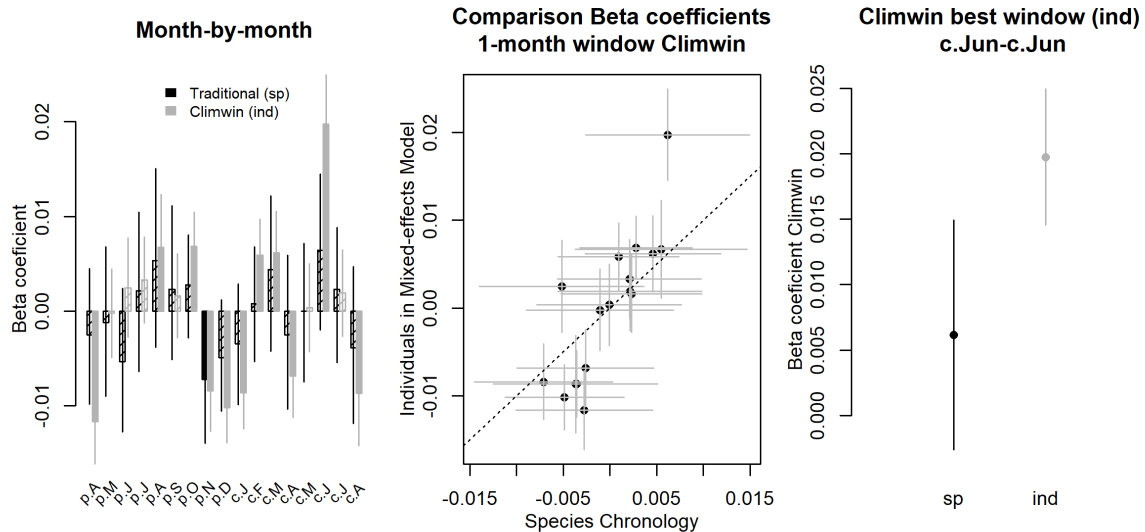


Figure S1. Comparison of our approach with traditional methods of identifying climate signals: LITU at SCBI. Shown are responses to the precipitation- and temperature-group variables selected as most influential by the *climwin* analysis. Left panels show a month-by-month comparison of *beta* (slope) coefficients for the relationship between tree growth and the monthly climate variable from species-level residual chronologies (traditional approach) and from individual-level analysis in *climwin* (approach presented here). Center panels compare the monthly *beta* coefficient estimates, with the dotted line indicating 1:1 correspondence. Finally, the right panels compare *beta* coefficients for the optimal window selected by *climwin*. Error bars indicate standard error of slope estimates. Note that 1:1 correspondence is not necessarily expected. See Appendix 5 for analysis methods and discussion of expected correspondence.

Figure S2. Comparison of our approach with traditional methods of identifying climate signals: ABAL at Zofin.

Precipitation Day Frequency



Maximum temperature

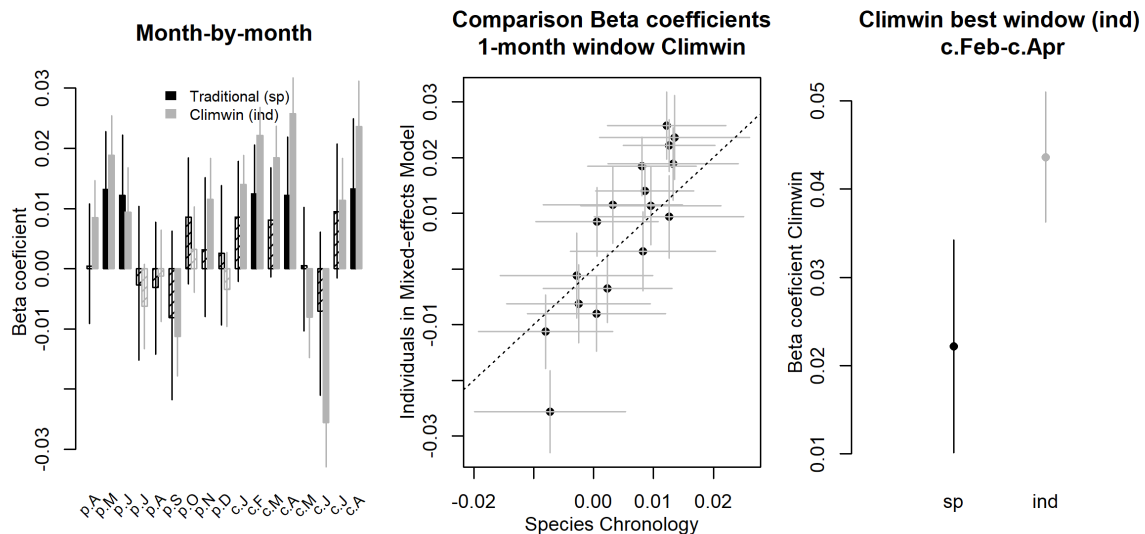
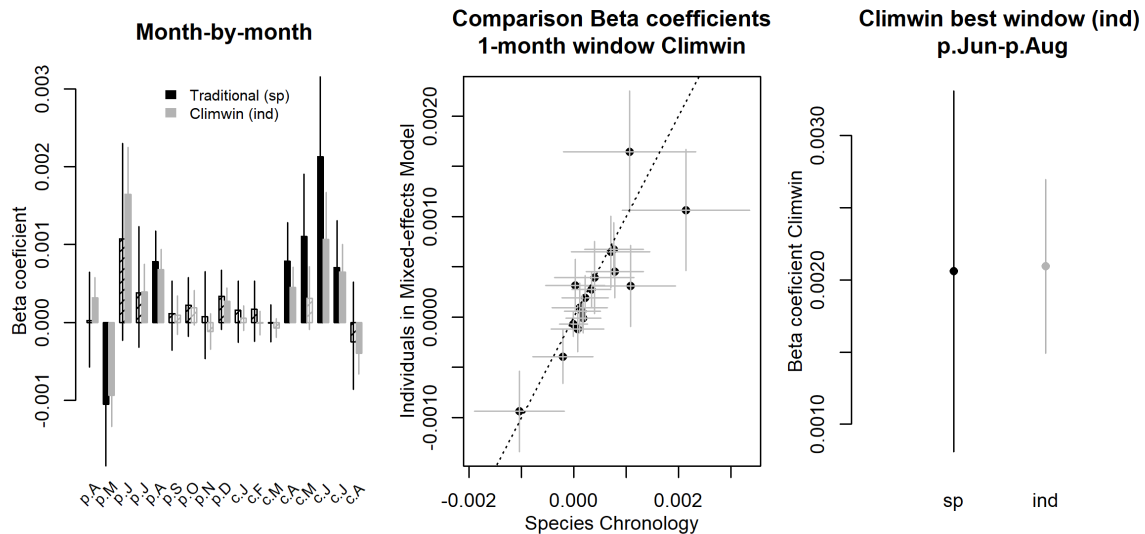


Figure S2. Comparison of our approach with traditional methods of identifying climate signals: ABAL at Zofin. Shown are responses to the precipitation- and temperature-group variables selected as most influential by the *climwin* analysis. Left panels show a month-by-month comparison of *beta* (slope) coefficients for the relationship between tree growth and the monthly climate variable from species-level residual chronologies (traditional approach) and from individual-level analysis in *climwin* (approach presented here). Center panels compare the monthly *beta* coefficient estimates, with the dotted line indicating 1:1 correspondence. Finally, the right panels compare *beta* coefficients for the optimal window selected by *climwin*. Error bars indicate standard error of slope estimates. Note that 1:1 correspondence is not necessarily expected. See Appendix 5 for analysis methods and discussion of expected correspondence.

Figure S3. Comparison of our approach with traditional methods of identifying climate signals: PSME at Cedar Breaks.

Precipitation



Maximum temperature

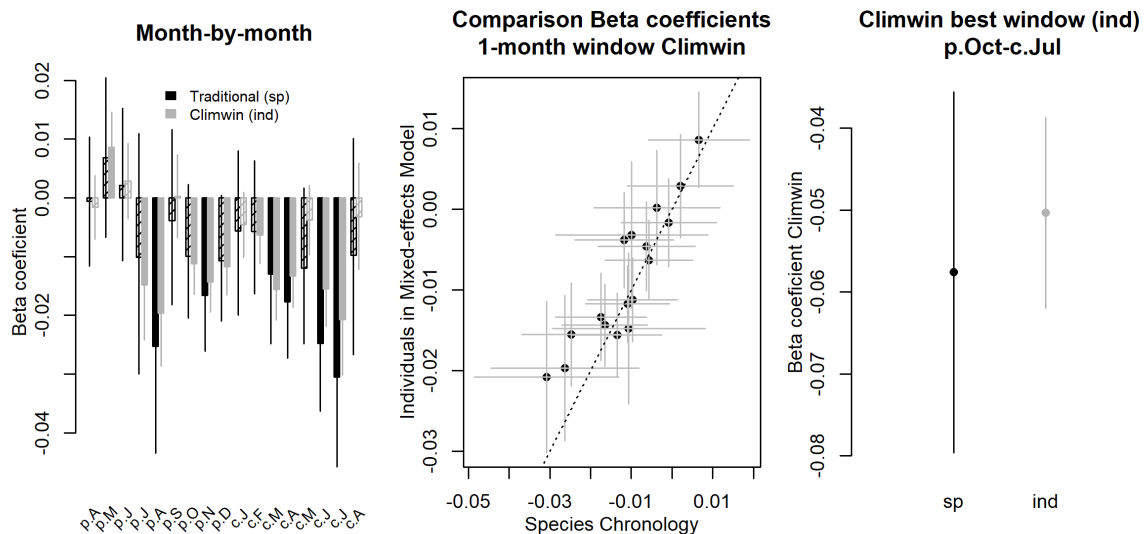
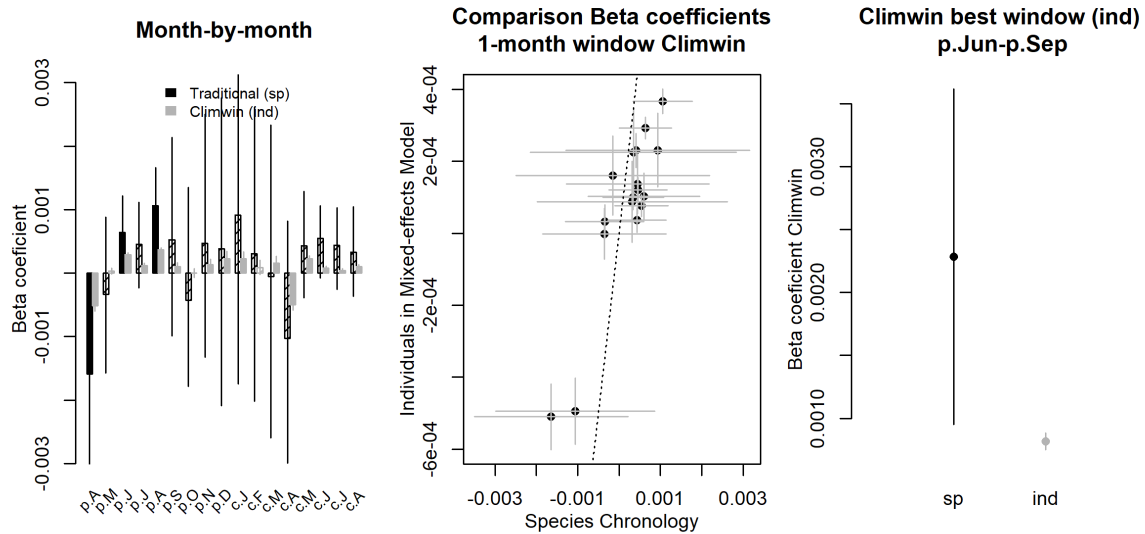


Figure S3. Comparison of our approach with traditional methods of identifying climate signals: PSME at Cedar Breaks. Shown are responses to the precipitation- and temperature-group variables selected as most influential by the *climwin* analysis. Left panels show a month-by-month comparison of *beta* (slope) coefficients for the relationship between tree growth and the monthly climate variable from species-level residual chronologies (traditional approach) and from individual-level analysis in *climwin* (approach presented here). Center panels compare the monthly *beta* coefficient estimates, with the dotted line indicating 1:1 correspondence. Finally, the right panels compare *beta* coefficients for the optimal window selected by *climwin*. Error bars indicate standard error of slope estimates. Note that 1:1 correspondence is not necessarily expected. See Appendix 5 for analysis methods and discussion of expected correspondence.

Figure S4. Comparison of our approach with traditional methods of identifying climate signals: PIMA at Scotty Creek.

Precipitation



Maximum temperature

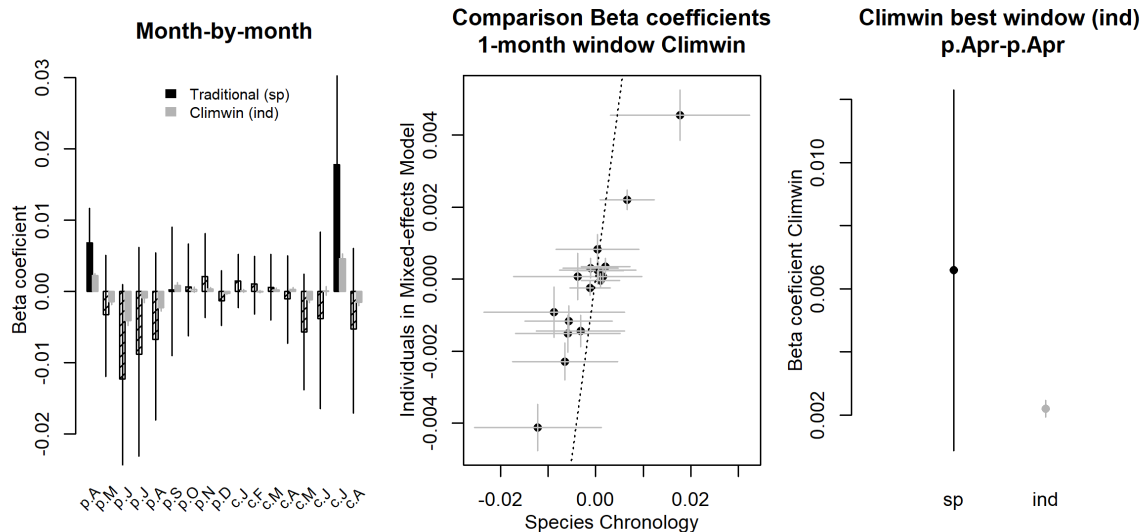


Figure S4. Comparison of our approach with traditional methods of identifying climate signals: PIMA at Scotty Creek. Shown are responses to the precipitation- and temperature-group variables selected as most influential by the *climwin* analysis. Left panels show a month-by-month comparison of *beta* (slope) coefficients for the relationship between tree growth and the monthly climate variable from species-level residual chronologies (traditional approach) and from individual-level analysis in *climwin* (approach presented here). Center panels compare the monthly *beta* coefficient estimates, with the dotted line indicating 1:1 correspondence. Finally, the right panels compare *beta* coefficients for the optimal window selected by *climwin*. Error bars indicate standard error of slope estimates. Note that 1:1 correspondence is not necessarily expected. See Appendix 5 for analysis methods and discussion of expected correspondence.

Figure S5. (PRE at SCBI)

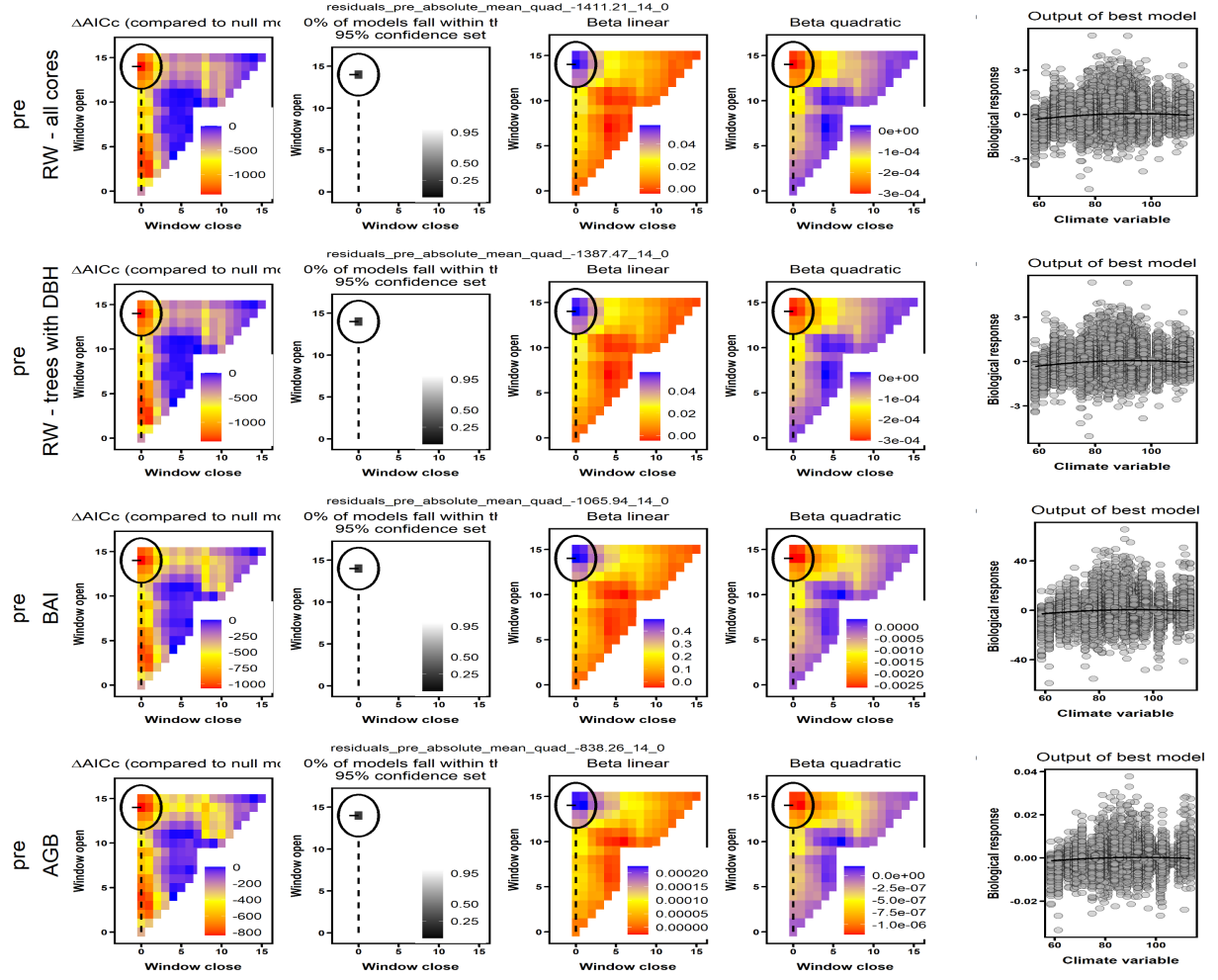


Figure S5. (PRE at SCBI) Here, *climwin* identified **GIVE WINDOW** precipitation (*PPT*) as the strongest climate variable across all four analyses (*RW* with and without trees for which *DBH* could not be reconstructed, *BAI*, ΔAGB).

Figure S6. (PET at SCBI)

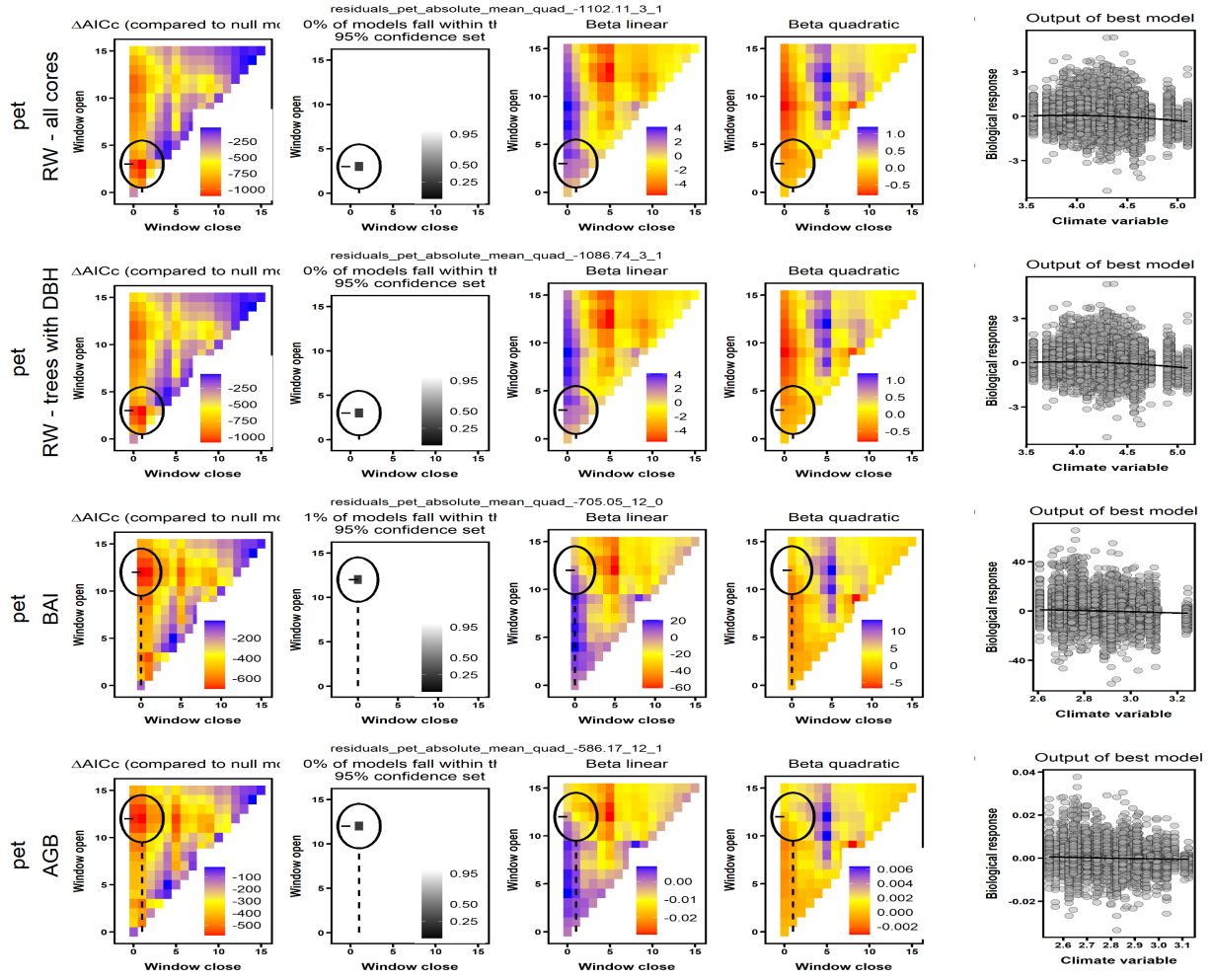


Figure S6. (PET at SCBI) Here, *climwin* identified potential evapotranspiration (PET) as the strongest climate variable across all four analyses (*RW* with and without trees for which *DBH* could not be reconstructed, *BAI*, ΔAGB), but a different window (**GIVE WINDOW**) was chosen for *BAI* and ΔAGB than for *RW* (**GIVE WINDOW**).

Figure S7. (TMP/TMN at BCI)

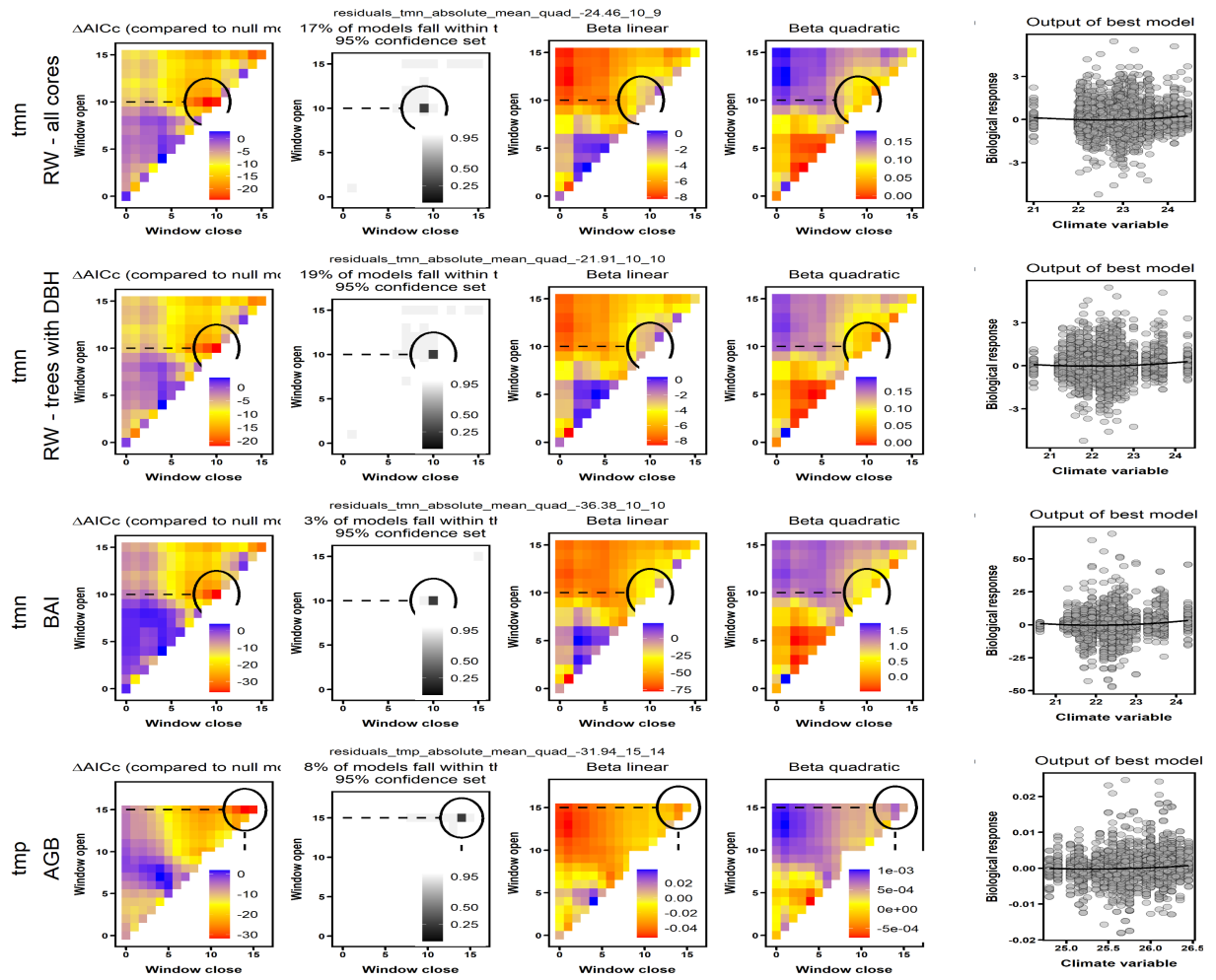


Figure S7. (TMP/TMN at BCI) Here....

Figure S9. Best GLS models for Barro Colorado Island (Panama)

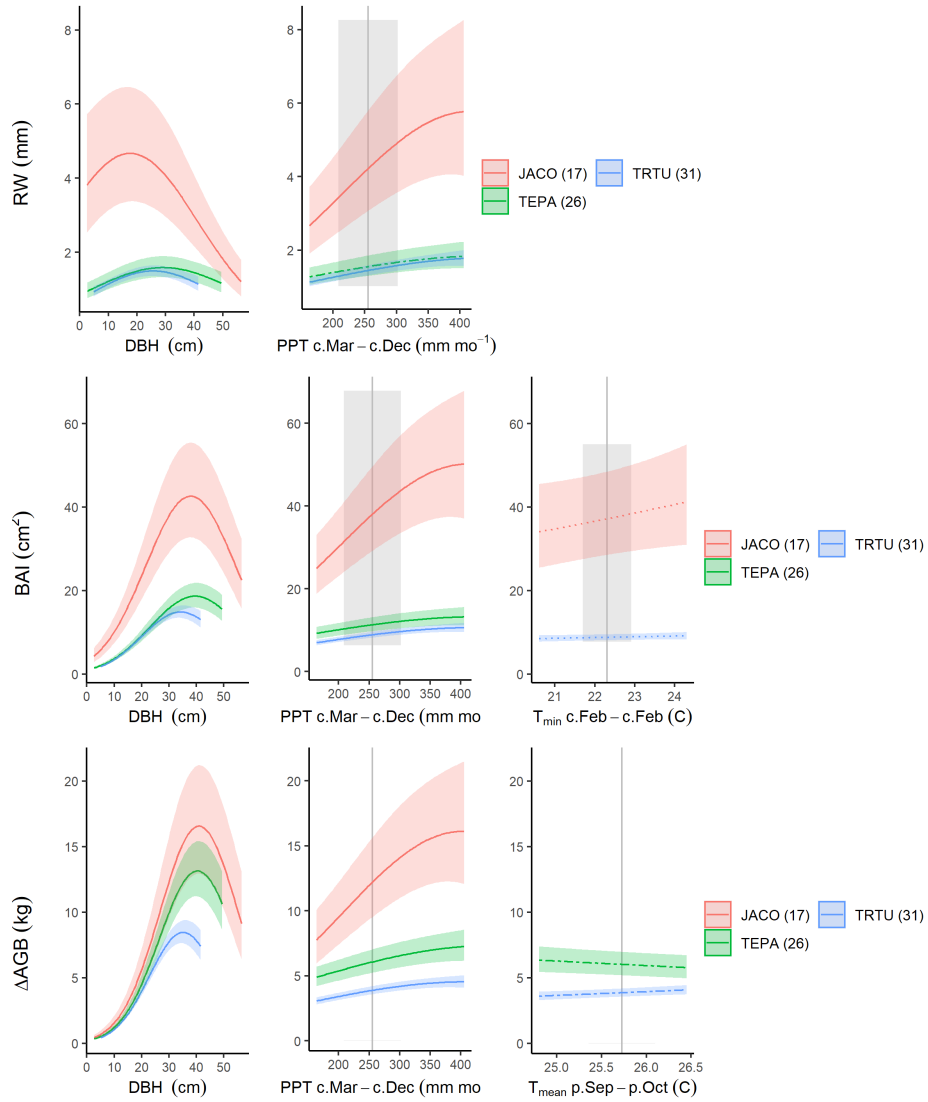


Figure S9. Best GLS models for Barro Colorado Island (Panama) for all three growth metrics examined here. Precipitation and temperature group variables are as selected by *climwin* (*p*=previous year, *c*=current year). For each species, relationships are plotted if included in top model, with best-fit polynomials plotted with solid lines when both first- and second-order terms are significant, dashed lines when only one term is significant, and dotted lines when neither is significant. Transparent ribbons indicate 95% confidence intervals. Vertical grey lines indicate the long-term mean for the climate variable, shading indicates 1 SD.

Figure S10. Best GLS models for Huai Kha Khaeng (Thailand)

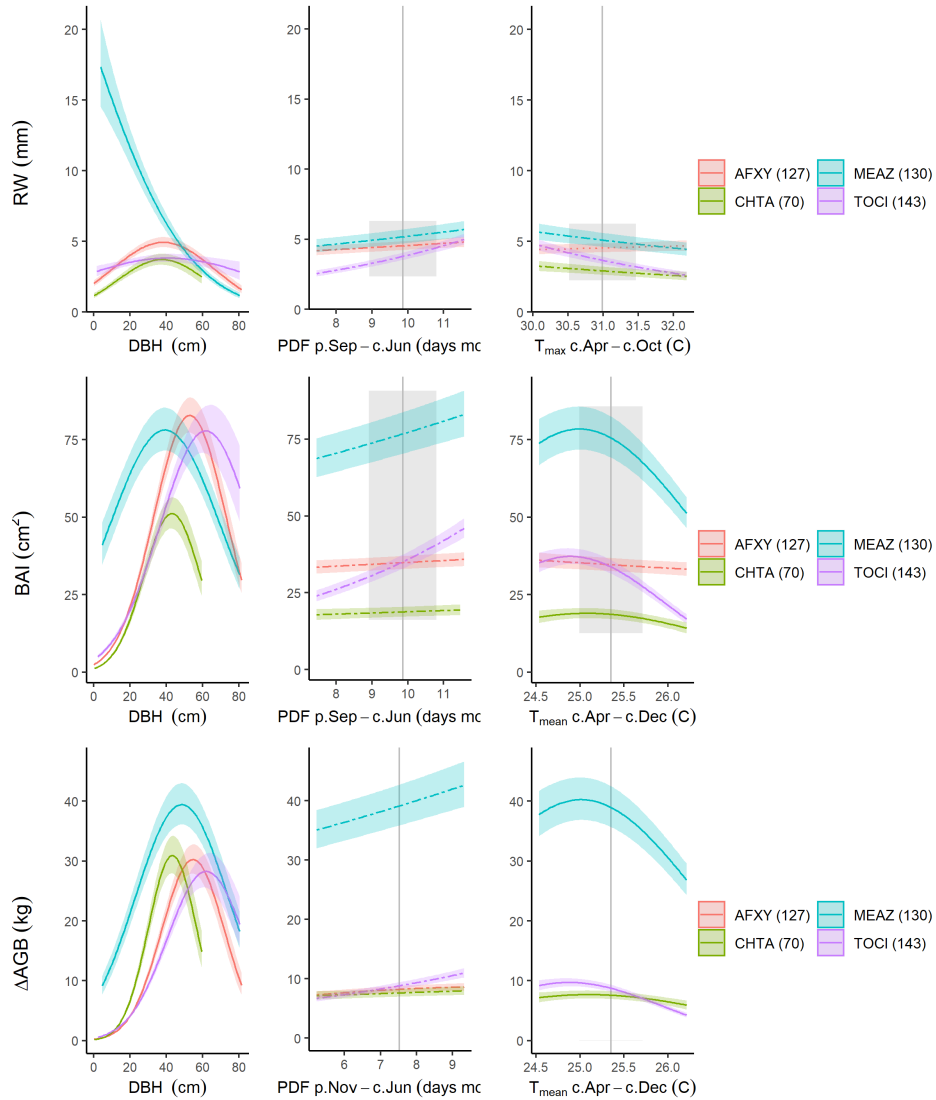


Figure S10. Best GLS models for Huai Kha Khaeng (Thailand) for all three growth metrics examined here. Precipitation and temperature group variables are as selected by *climwin* (*p*=previous year, *c*=current year). For each species, relationships are plotted if included in top model, with best-fit polynomials plotted with solid lines when both first- and second-order terms are significant, dashed lines when only one term is significant, and dotted lines when neither is significant. Transparent ribbons indicate 95% confidence intervals. Vertical grey lines indicate the long-term mean for the climate variable, shading indicates 1 SD.

Figure S11. Best GLS models for the Smithsonian Conservation Biology Institute (Virginia, USA)

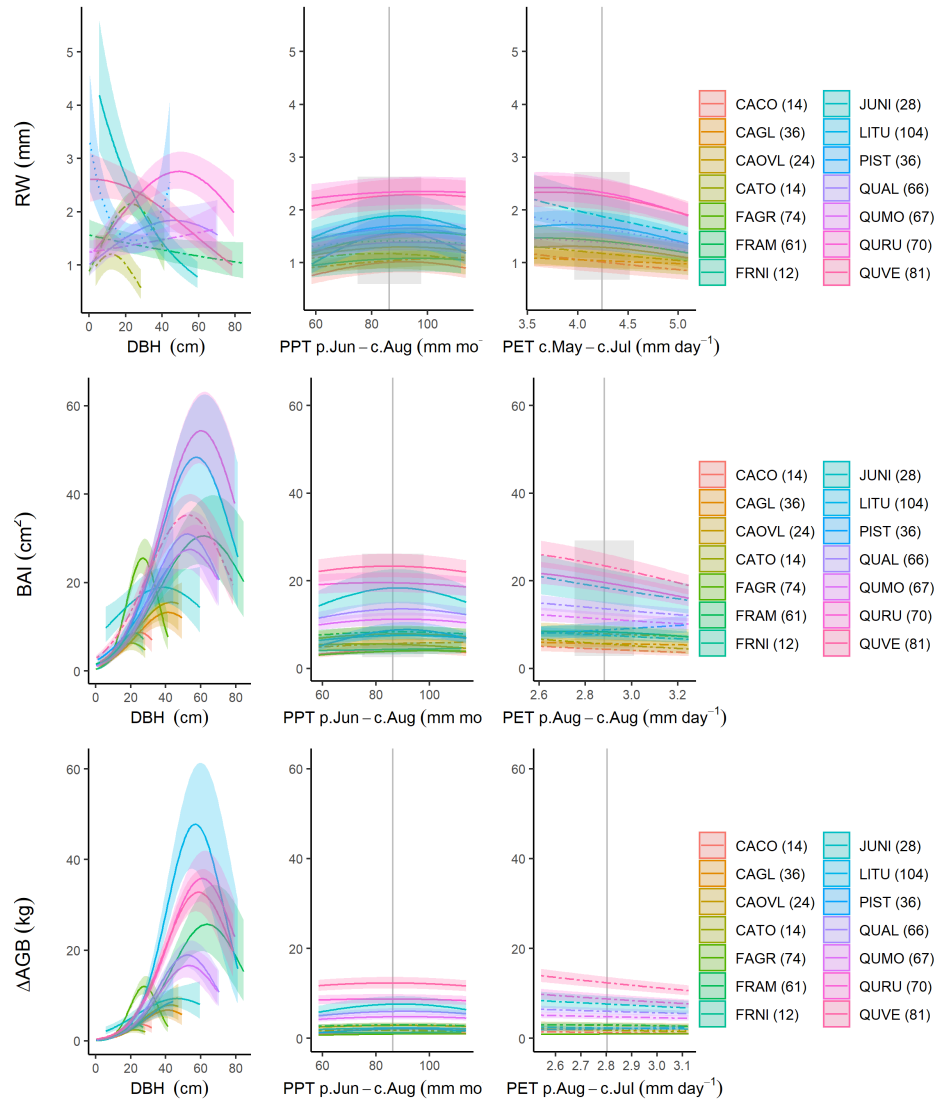


Figure S11. Best GLS models for the Smithsonian Conservation Biology Institute (Virginia, USA) for all three growth metrics examined here. Precipitation and temperature group variables are as selected by *climwin* (*p*=previous year, *c*=current year). For each species, relationships are plotted if included in top model, with best-fit polynomials plotted with solid lines when both first- and second-order terms are significant, dashed lines when only one term is significant, and dotted lines when neither is significant. Transparent ribbons indicate 95% confidence intervals. Vertical grey lines indicate the long-term mean for the climate variable, shading indicates 1 SD.

Figure S12. Best GLS models for Lilley Dickey Woods (Indiana, USA)

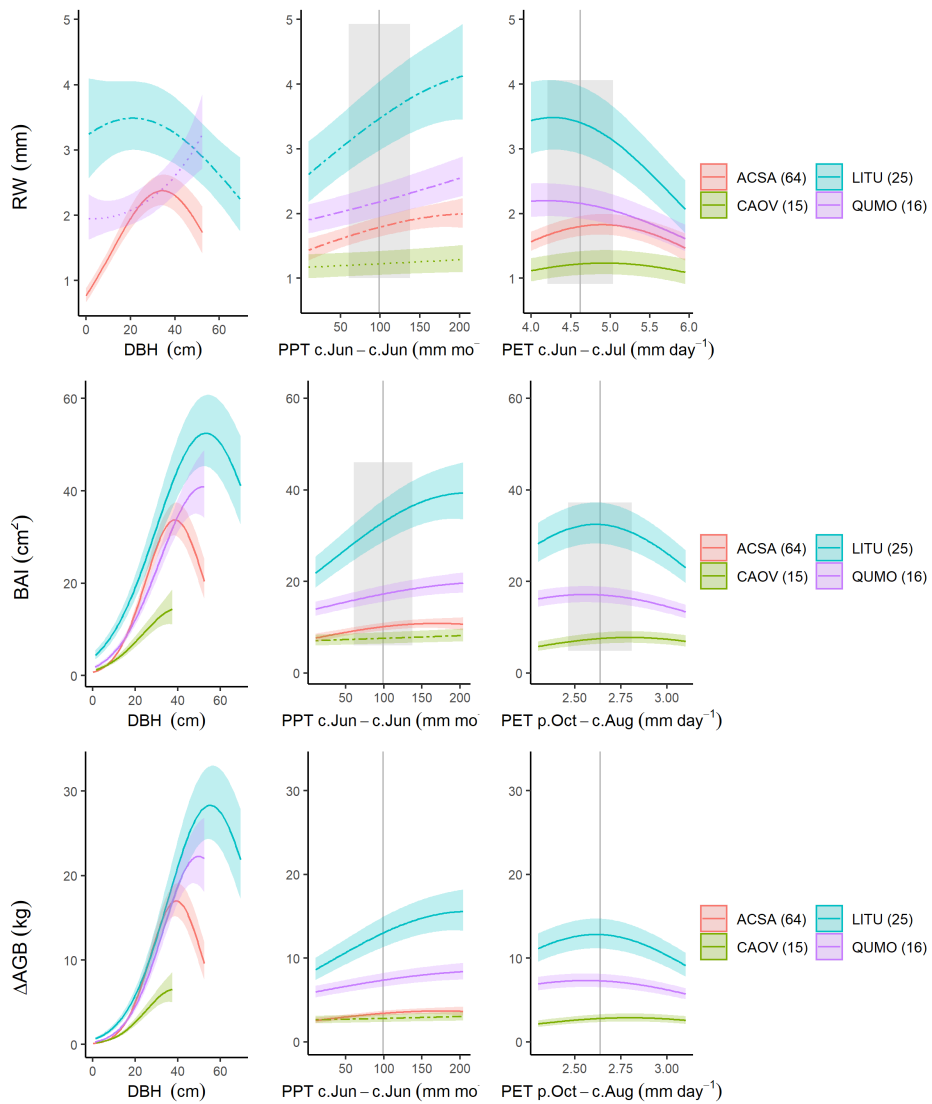


Figure S12. Best GLS models for Lilley Dickey Woods (Indiana, USA) for all three growth metrics examined here. Precipitation and temperature group variables are as selected by *climwin* (*p*=previous year, *c*=current year). For each species, relationships are plotted if included in top model, with best-fit polynomials plotted with solid lines when both first- and second-order terms are significant, dashed lines when only one term is significant, and dotted lines when neither is significant. Transparent ribbons indicate 95% confidence intervals. Vertical grey lines indicate the long-term mean for the climate variable, shading indicates 1 SD.

Figure S13. Best GLS models for Harvard Forest (Massachusetts, USA)

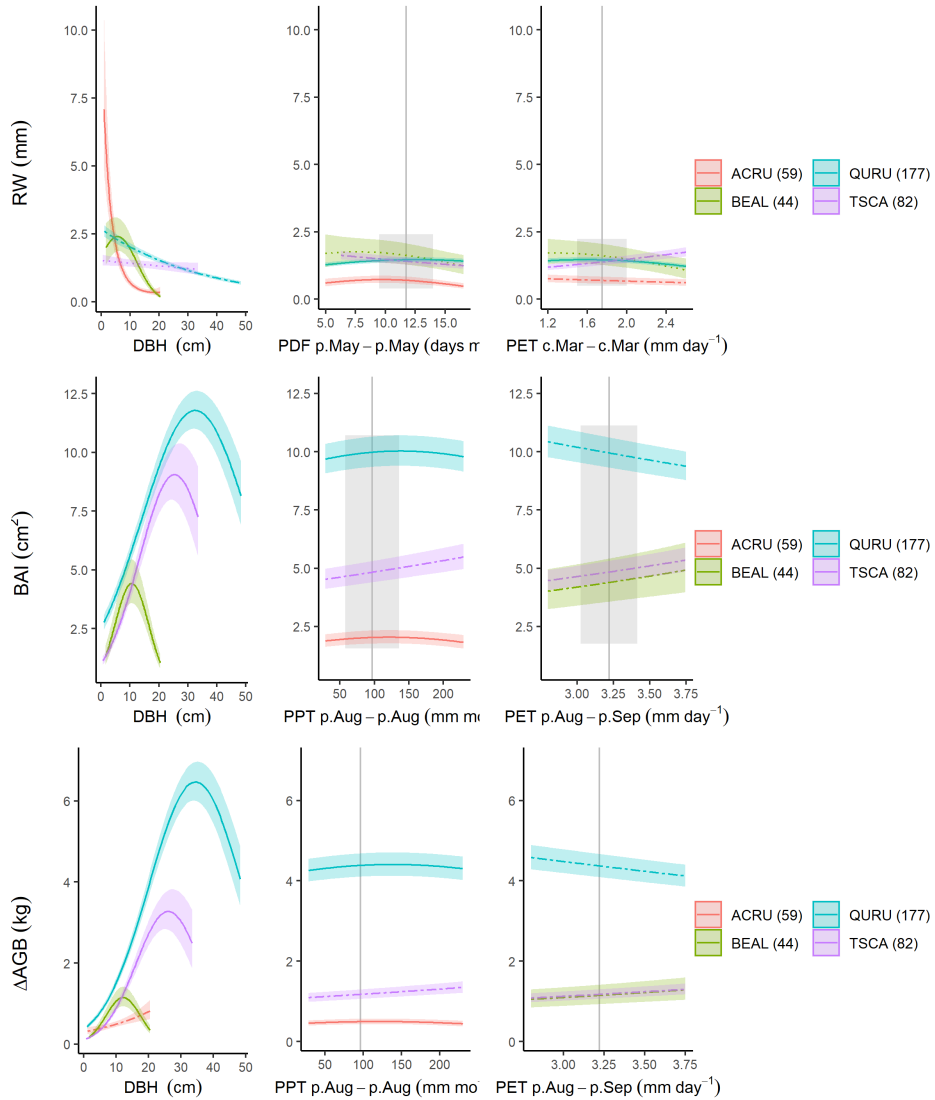


Figure S13. Best GLS models for Harvard Forest (Massachusetts, USA) for all three growth metrics examined here. Precipitation and temperature group variables are as selected by *climwin* (*p*=previous year, *c*=current year). For each species, relationships are plotted if included in top model, with best-fit polynomials plotted with solid lines when both first- and second-order terms are significant, dashed lines when only one term is significant, and dotted lines when neither is significant. Transparent ribbons indicate 95% confidence intervals. Vertical grey lines indicate the long-term mean for the climate variable, shading indicates 1 SD.

Figure S14. Best GLS models for Zofin Forest (Czech Republic)

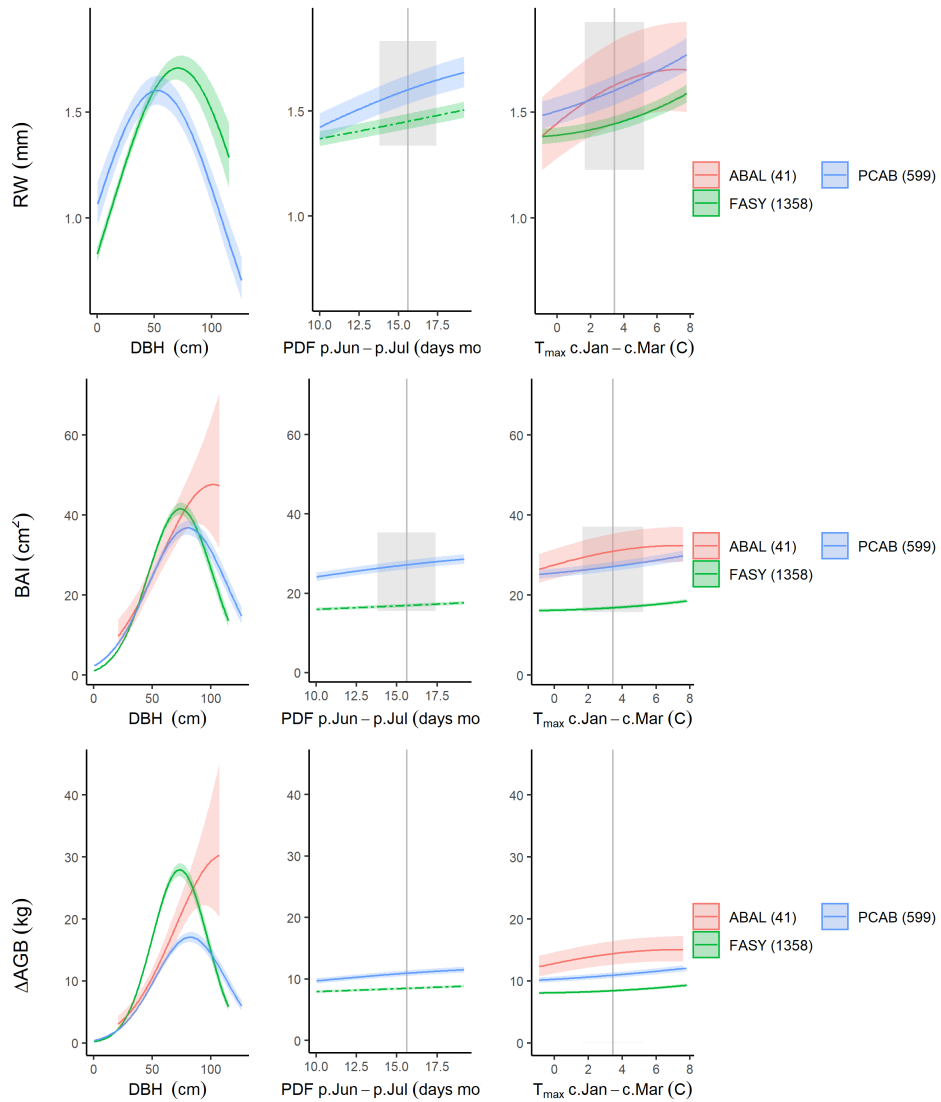


Figure S14. Best GLS models for Zofin Forest (Czech Republic) for all three growth metrics examined here. Precipitation and temperature group variables are as selected by *climwin* (*p*=previous year, *c*=current year). For each species, relationships are plotted if included in top model, with best-fit polynomials plotted with solid lines when both first- and second-order terms are significant, dashed lines when only one term is significant, and dotted lines when neither is significant. Transparent ribbons indicate 95% confidence intervals. Vertical grey lines indicate the long-term mean for the climate variable, shading indicates 1 SD.

Figure S15. Best GLS models for Niobrara/ Halsey (Nebraska, USA)

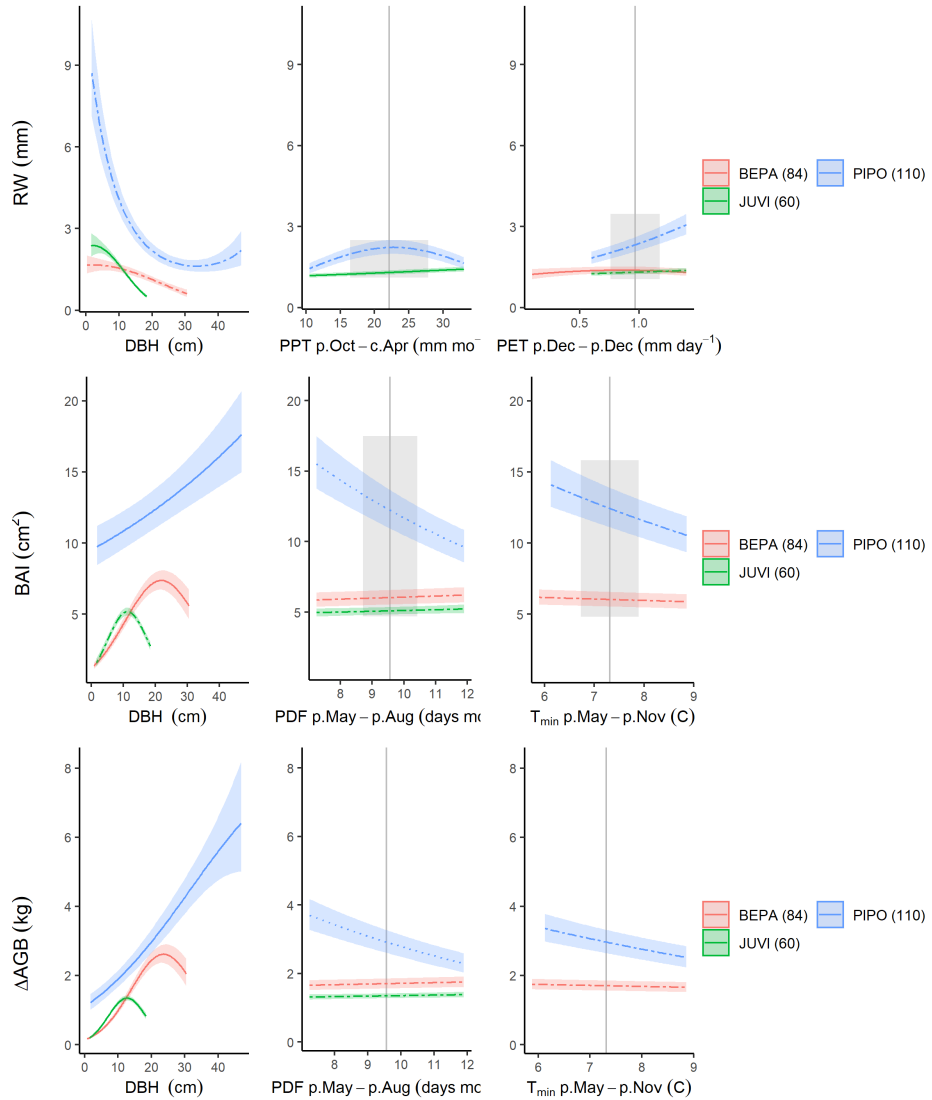


Figure S15. Best GLS models for Niobrara/ Halsey (Nebraska, USA) for all three growth metrics examined here. Precipitation and temperature group variables are as selected by *climwin* (*p*=previous year, *c*=current year). For each species, relationships are plotted if included in top model, with best-fit polynomials plotted with solid lines when both first- and second-order terms are significant, dashed lines when only one term is significant, and dotted lines when neither is significant. Transparent ribbons indicate 95% confidence intervals. Vertical grey lines indicate the long-term mean for the climate variable, shading indicates 1 SD.

Figure S16. Best GLS models for Little Tesuque (New Mexico, USA)

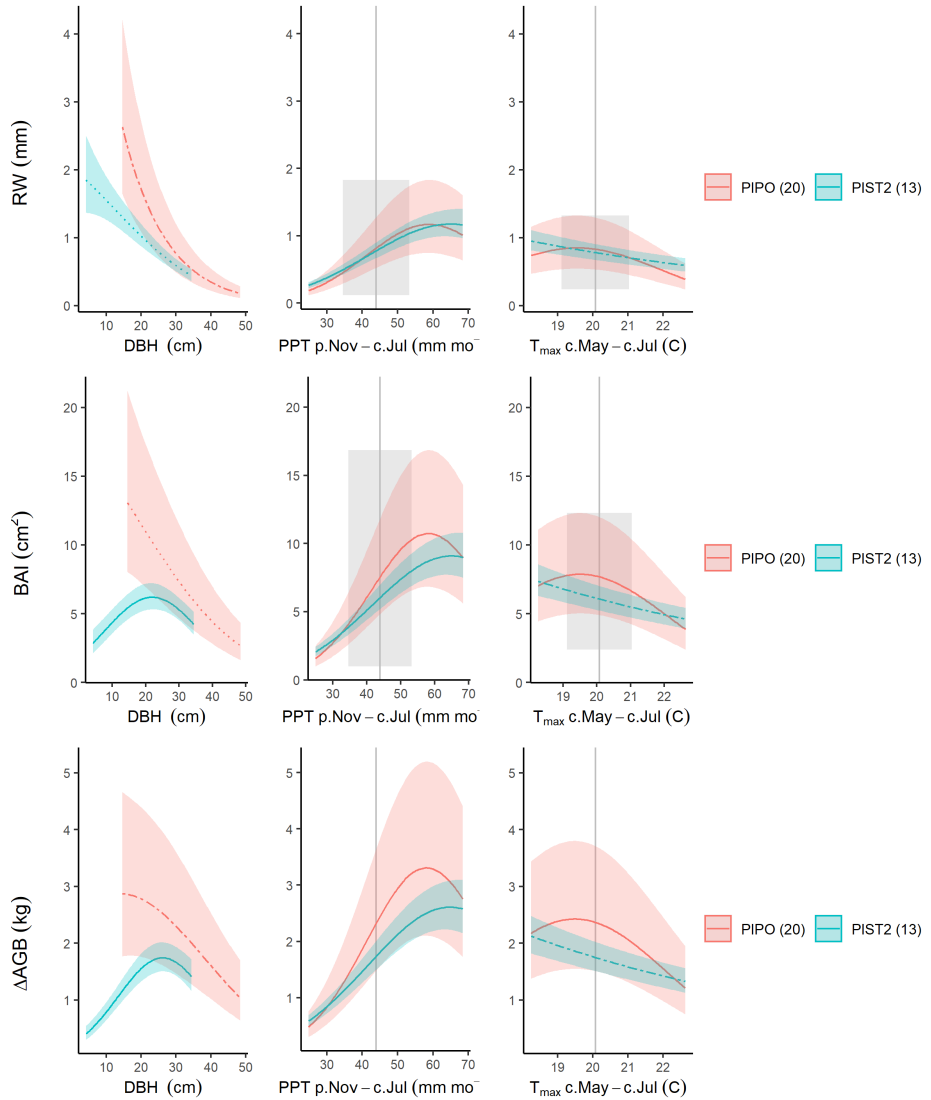


Figure S16. Best GLS models for Little Tesuque (New Mexico, USA) for all three growth metrics examined here. Precipitation and temperature group variables are as selected by *climwin* (*p*=previous year, *c*=current year). For each species, relationships are plotted if included in top model, with best-fit polynomials plotted with solid lines when both first- and second-order terms are significant, dashed lines when only one term is significant, and dotted lines when neither is significant. Transparent ribbons indicate 95% confidence intervals. Vertical grey lines indicate the long-term mean for the climate variable, shading indicates 1 SD.

Figure S17. Best GLS models for Cedar Breaks (Utah, USA)

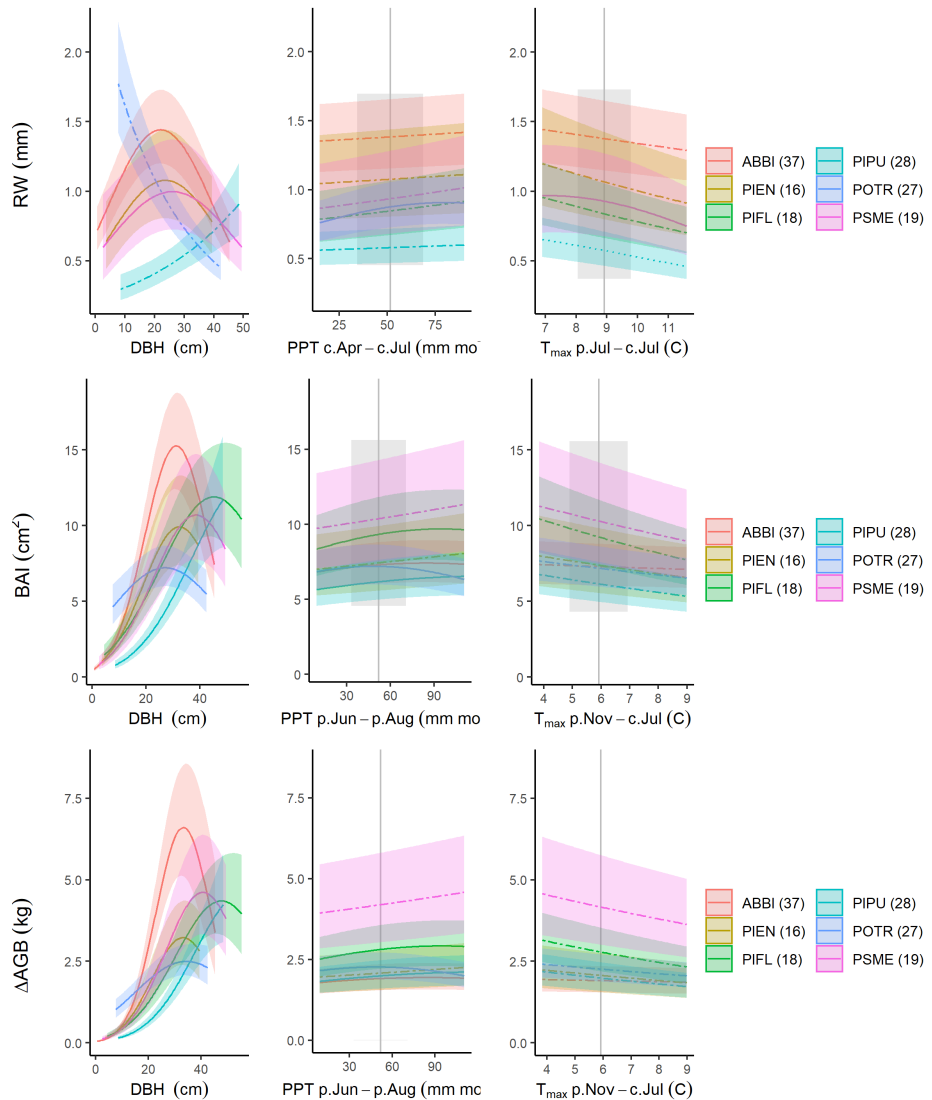


Figure S17. Best GLS models for Cedar Breaks (Utah, USA) for all three growth metrics examined here. Precipitation and temperature group variables are as selected by *climwin* (*p*=previous year, *c*=current year). For each species, relationships are plotted if included in top model, with best-fit polynomials plotted with solid lines when both first- and second-order terms are significant, dashed lines when only one term is significant, and dotted lines when neither is significant. Transparent ribbons indicate 95% confidence intervals. Vertical grey lines indicate the long-term mean for the climate variable, shading indicates 1 SD.

Figure S18. Best GLS models for Scotty Creek (Northwest Territory, Canada)

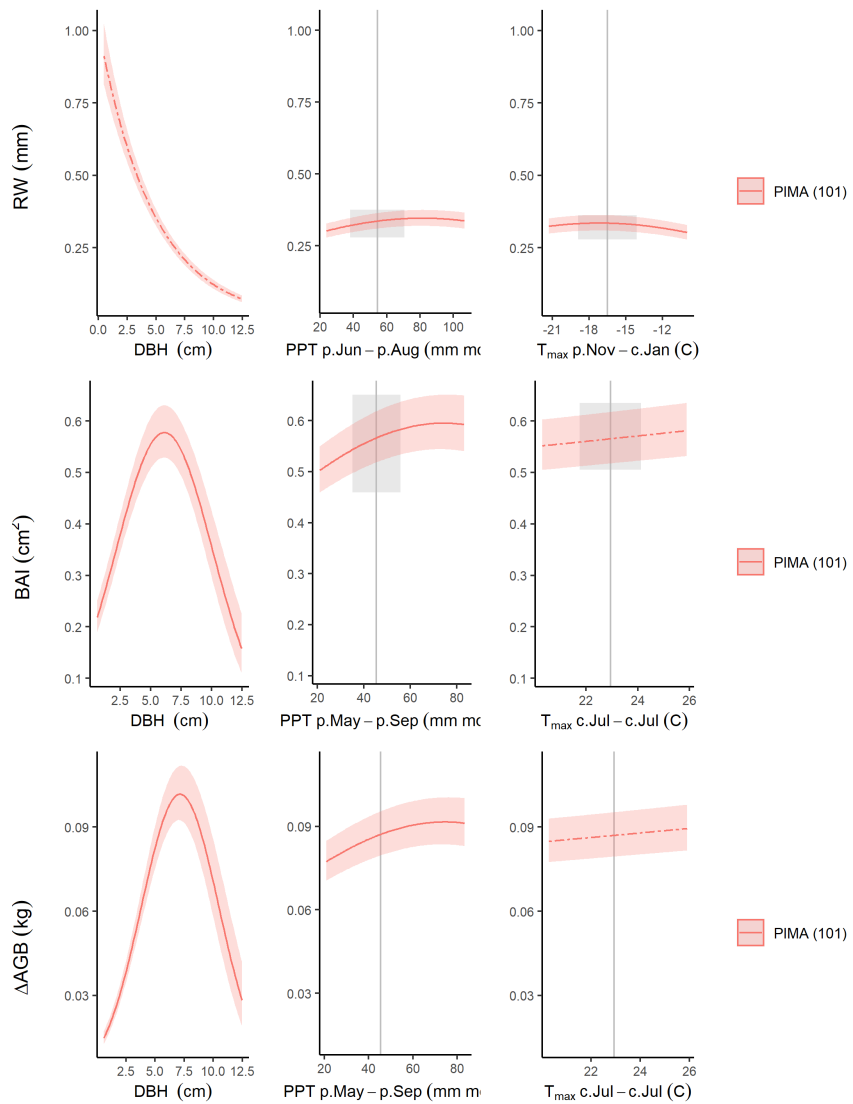


Figure S18. Best GLS models for Scotty Creek (Northwest Territory, Canada) for all three growth metrics examined here. Precipitation and temperature group variables are as selected by *climwin* (*p*=previous year, *c*=current year). For each species, relationships are plotted if included in top model, with best-fit polynomials plotted with solid lines when both first- and second-order terms are significant, dashed lines when only one term is significant, and dotted lines when neither is significant. Transparent ribbons indicate 95% confidence intervals. Vertical grey lines indicate the long-term mean for the climate variable, shading indicates 1 SD.

SI References

- Applequist, M. (1958). A simple pith locator for use with off-center increment cores. *Journal of Forestry*.
- Aus de Ar, R. (2018). Tree Rings of *Pinus ponderosa* and *Juniperus virginiana* Show Different Responses to Stand Density and Water Availability in the Nebraska Grasslands. *The American Midland Naturalist*, 180(1), 18. <https://doi.org/10.1674/0003-0031-180.1.18>
- Bumann, E., Awada, T., Wardlow, B., Hayes, M., Okalebo, J., Helzer, C., Mazis, A., Hiller, J., & Cherubini, P. (2019). Assessing responses of *Betula Papyrifera* to climate variability in a remnant population along the Niobrara River Valley in Nebraska, U.S.A., Through dendroecological and remote-sensing techniques. *Canadian Journal of Forest Research*, 49(5), 423–433. <https://doi.org/10.1139/cjfr-2018-0206>
- Charney, N. D., Babst, F., Poulter, B., Record, S., Trouet, V. M., Frank, D., Enquist, B. J., & Evans, M. E. K. (2016). Observed forest sensitivity to climate implies large changes in 21st century North American forest growth. *Ecology Letters*, 19(9), 1119–1128. <https://doi.org/10.1111/ele.12650>
- Duncan, R. P. (1989). An evaluation of errors in tree age estimates based on increment cores in kahikatea (*Dacrycarpus dacrydioides*). *New Zealand Natural Sciences*, 16, 31–37.
- Helcoski, R., Tepley, A. J., Pederson, N., McGarvey, J. C., Meakem, V., Herrmann, V., Thompson, J. R., & Anderson-Teixeira, K. J. (2019). Growing season moisture drives interannual variation in woody productivity of a temperate deciduous forest. *New Phytologist*, 223(3), 1204–1216. <https://doi.org/10.1111/nph.15906>
- Kašpar, K., Tumajer, J., Vašíčková, I., & Šamonil, P. (n.d.). *Species-specific climate-growth interactions determine the future tree species dynamics of the mixed Central European mountain forests*.
- Maxwell, J. T., Harley, G. L., & Robeson, S. M. (2016). On the declining relationship between tree growth and climate in the Midwest United States: The fading drought signal. *Climatic Change*, 138(1-2), 127–142. <https://doi.org/10.1007/s10584-016-1720-3>
- Paton, S. (2019). *Barro Colorado Island, Clearing_Precipitation, manual*. The Smithsonian Institution. <https://doi.org/10.25573/data.10042502.v3>
- Sniderhan, A. E., & Baltzer, J. L. (2016). Growth dynamics of black spruce (*Picea Mariana*) in a rapidly thawing discontinuous permafrost peatland: Growth Dynamics Boreal Peatlands. *Journal of Geophysical Research: Biogeosciences*, 121(12), 2988–3000. <https://doi.org/10.1002/2016JG003528>
- Tumajer, J., Altman, J., Štěpánek, P., Treml, V., Doležal, J., & Cienciala, E. (2017). Increasing moisture limitation of Norway spruce in Central Europe revealed by forward modelling of tree growth in tree-ring network. *Agricultural and Forest Meteorology*, 247, 56–64. <https://doi.org/10.1016/j.agrformet.2017.07.015>
- Vlam, M., Baker, P. J., Bunyavejchewin, S., & Zuidema, P. A. (2014). Temperature and rainfall strongly drive temporal growth variation in Asian tropical forest trees. *Oecologia*, 174(4), 1449–1461. <https://doi.org/10.1007/s00442-013-2846-x>
- Williams, A. P., Allen, C. D., Macalady, A. K., Griffin, D., Woodhouse, C. A., Meko, D. M., Swetnam, T. W., Rauscher, S. A., Seager, R., Grissino-Mayer, H. D., Dean, J. S., Cook, E. R., Gangodagamage, C., Cai, M., & McDowell, N. G. (2012). Temperature as a potent driver of regional forest drought stress and tree mortality. *Nature Climate Change*. <https://doi.org/10.1038/nclimate1693>